Article:

Yun, X., Zhu, Y. orcid.org/0000-0003-4818-8359, Meng, X. et al. (1 more author) (2023) Welded steel I-section columns: residual stresses, testing, simulation and design. Engineering Structures, 282. 115631. ISSN 0141-0296

https://doi.org/10.1016/j.engstruct.2023.115631

Yun X, Zhu YF, Meng X, Gardner L (2023). Welded steel I-section columns: Residual stresses, testing, simulation and design. Engineering Structures, 282, 115631.

Welded steel I-section columns: Residual stresses, testing, simulation and design

Xiang Yun[1], Yufei Zhu[2], Xin Meng[2] and Leroy Gardner[2]

[1]*Department of Civil and Structural Engineering, The University of Sheffield, Sheffield S1 3JD, UK*
[2]*Department of Civil and Environmental Engineering, Imperial College London, London SW7 2AZ, UK*

Abstract: The flexural buckling behaviour and design of homogeneous and hybrid welded I-section columns, considering a wide range of steel grades, are investigated in the present study. Residual stresses are first examined through the statistical analysis of 71 existing experimental results collected from the literature; on the basis of the findings, a new residual stress model for S235 to S960 steel welded I-sections is proposed. Experiments on a total of five pin-ended homogeneous (S690) and hybrid (S355 web and S690 flanges) welded I-section columns buckling about the major axis are then presented. In parallel with the experimental programme, finite element (FE) models were created and validated against the experimental results obtained from the present study, as well as those collected from the literature. The developed FE models were shown to be capable of accurately replicating the key experimental responses, and were then utilised to carry out extensive parametric studies, through which additional 6000 numerical column buckling data covering a wide range of steel grades, cross-section geometries and member slendernesses were generated. The combined experimental and numerical data were used to evaluate the accuracy of the flexural buckling design rules for welded I-section columns set out in the current European and North American design standards, where shortcomings relating to the consideration of steel grade were identified. A modified Eurocode 3 (EC3) method was devised to reflect the influence of yield strength on the buckling resistances of welded I-section columns more systematically and shown to provide substantially improved resistance predictions in terms of accuracy and consistency; the reliability of the modified approach was statistically verified following the procedure set out in

Annex D of EN 1990 and is considered to be suitable for incorporation into future revisions of Eurocode 3.

Keywords: Column buckling tests; Design methods; Finite element modelling; High strength steels; Hybrid sections; Member stability; Residual stresses; Welded I-sections.

1. Introduction

Structural steel welded I-section members are commonly used in the construction industry, and are typically fabricated from normal strength steel (NSS) plates. High strength steel (HSS) and hybrid (NSS web and HSS flanges) welded I-section columns are examined in the present study, seeking to promote more cost-effective, sustainable and lightweight structural solutions. To date, a number of experimental studies have been carried out to investigate the minor axis flexural buckling behaviour of homogeneous HSS (i.e. with nominal yield strengths greater than or equal to 460 MPa) welded I-section columns, such as those reported in [1-4], while only a few studies have focused on buckling about the major axis [5,6]. The previous investigations have shown that HSS welded I-section columns generally exhibit superior normalised flexural buckling resistances relative to their normal strength steel (NSS) counterparts, and that current stability design provisions tend to be rather conservative. With regards to hybrid welded I-sections, which are able to provide more cost-effective design solutions for structural elements that are primarily subjected to bending (e.g. beams and beam-columns) than their homogenous HSS counterparts, although experimental studies have been carried out to investigate their local [7-9] and lateral torsional [10,11] buckling behaviour, there appears to have been no research into their flexural buckling performance. Further experimental investigations into the flexural buckling behaviour of both homogeneous and hybrid welded I-section columns, especially considering buckling about the major axis, are therefore deemed necessary.

Regarding the stability design of welded I-section structural elements, the European design codes (i.e. the current version of EN 1993-1-1 [12] and EN 1993-1-12 [13] as well as the latest draft version of prEN 1993-1-1 [14]) are applicable to the design of homogeneous welded I-section columns made of steel grades up to S700, while the current American specification AISC 360 [15] provides design rules for homogeneous welded I-section columns with nominal yield strengths up to 690 N/mm^2. However, none of the current specifications cover the design of homogeneous welded I-section columns made of ultra HSS grades (e.g. S960) or hybrid welded I-section columns consisting of higher strength steel flanges and a lower strength steel web. In addition, the existing design provisions generally prescribe a single buckling curve for the flexural buckling design of welded I-sections made of varying steel grades [15], or have a step-wise change of buckling curve at a specified steel strength [12-14]. Neither reflects the true, gradual influence of steel strength (and associated residual stresses) on the flexural buckling behaviour of columns [16,17].

The flexural buckling resistances of welded I-section columns can be strongly affected by residual stresses. Measurements of residual stresses in both NSS and HSS welded I-sections have been carried out in a number of previous studies [18-21], resulting in the proposal of different residual stress predictive models with varying complexity. It has been shown that the amplitudes of residual stresses in welded I-sections decrease as a proportion of the yield strength with increasing steel grade. A review of residual stress measurements and models for welded steel I-sections has been made by Tankova et al. [22]; on the basis of the collected residual stress measurements, statistical values of the amplitudes of residual stresses in welded I-sections with varying steel grades have also been provided. More recently, Schaper et al. [23] performed residual stress measurements on mono- and doubly-symmetric welded I-sections with steel grades ranging from S355 to S690, and proposed a new residual stress model that considers both cross-section geometry and steel grade. The residual stress amplitudes employed in the new model [23] correspond approximately to the mean values of the residual stress amplitudes in compression. An alternative approach is taken in the present paper – a residual stress model with two alternative residual stress amplitudes is proposed. The first model is based on mean residual stress values and is considered suitable for FE model validation; the second is based on characteristic (95 percentile) residual stress values and is considered suitable for FE parametric studies and design. This is consistent with the approach taken for initial geometric imperfections, whereby mean (measured) values are typically used for FE model validation and tolerance-based values are used in parametric studies and design.

This paper aims to characterise the flexural buckling behaviour and resistance of both homogeneous and hybrid welded I-section columns with varying steel grades through both experimental and numerical studies. Measured residual stress data from the literature were firstly collected and analysed to develop the above-mentioned residual stress model. An experimental programme was then conducted to generate flexural buckling data on homogeneous and hybrid welded I-section columns buckling about the major axis; a comprehensive numerical investigation to generate further column flexural buckling resistance data over a broader variety of steel grades, cross-section geometries and member slendernesses followed. The obtained test and numerical data were utilised to examine the accuracy and applicability of the codified column design rules, as specified in prEN 1993-1-1 [14] and AISC 360 [15], for both homogeneous and hybrid welded I-section columns. Finally, new design proposals were made to improve the accuracy and consistency of the flexural buckling resistance predictions; the reliability of the new design approach was verified by means of reliability analyses.

2. Residual stress model

Residual stresses are introduced into welded I-sections due primarily to the non-uniform cooling that takes place during and after the welding process. In this section, existing residual stress measurement data on doubly symmetric welded I-sections made of steel plates with nominal yield strengths ranging from 235 MPa to 960 MPa are analysed; the data collected from the literature [19-35] are summarised in Table 1.

Table 1. Existing residual stress measurements on doubly symmetric welded I-sections

Nominal yield strength (MPa)	No. of tests	Member type	Reference
235	1	Prismatic	Wang and Qin [24]
	3	Tapered	Shiomi and Kurata [25]
345/355/350	4	Tapered	Tankova et al. [22]
	4	Prismatic	Unsworth et al. [26]
	4	Prismatic	Yang et al. [27]
	7	Prismatic	Schaper et al. [28]
460	8	Prismatic	Ban et al. [29]
	8	Prismatic	Yang et al. [30]
	2	Prismatic	Schaper et al. [28]
	2	Prismatic	Tankova et al. [31]
	2	Prismatic	Zhao and Ding [32]
690	2	Prismatic	Sun et al. [33]
	1	Prismatic	Le et al. [19]
	4	Prismatic	Liu and Chung [20]
	3	Prismatic	Li et al. [21]
	1	Prismatic	Su et al. [34]
	4	Prismatic	Tankova et al. [31]
	5	Prismatic	Schaper et al. [23]
890	1	Prismatic	Le et al. [19]
960	3	Prismatic	Ban [35]
S690 (flange) + S355 (web)	2	Prismatic	Schaper et al. [23]

The collected measured residual stress data for doubly symmetric welded I-sections made of S355, S460 and S690 steels are presented in a normalised fashion in Figs. 1(a)-(c), where the measured residual stresses σ_r are normalised by their corresponding yield strengths f_y and plotted against the normalised positions with respect to the flange width or web depth of the measured welded I-section. Note that in Figs. 1(a)-(c), the origin of the horizontal axis corresponds to the web-to-flange junction while the value of 0.5 represents the location of the flange tip or the mid-height of the web of the measured welded I-section. Also note that throughout the present study positive values indicate tensile residual stresses while the negative values indicate compressive residual stresses. Moving averages over 40 adjacent data points of measured residual stresses for each considered steel grade are also plotted in Figs. 1(a)-(c), together with the ECCS model [36,37] and the predictive model for welded I-sections made of non-thermally cut plates recently proposed by Schaper et al. [23].

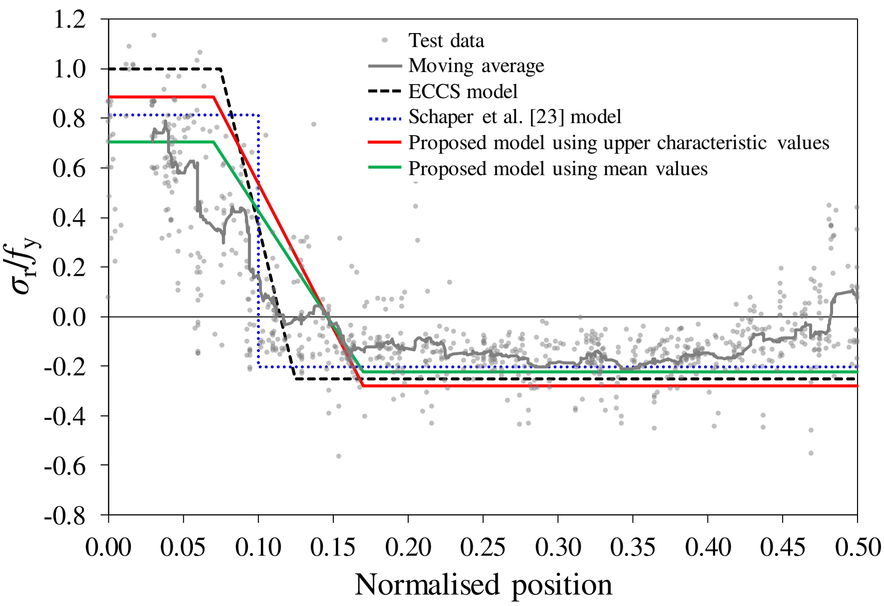

(a) S355 steel welded I-sections

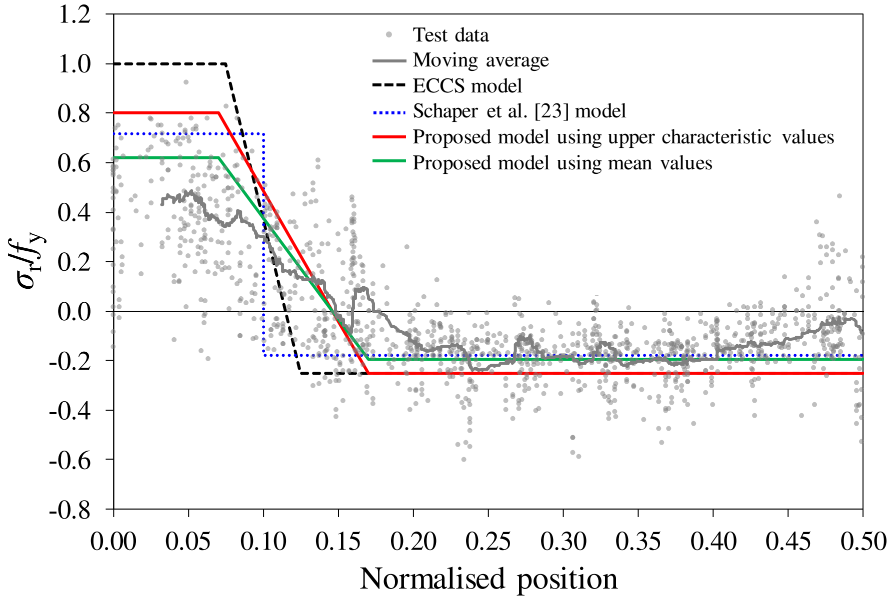

(b) S460 steel welded I-sections

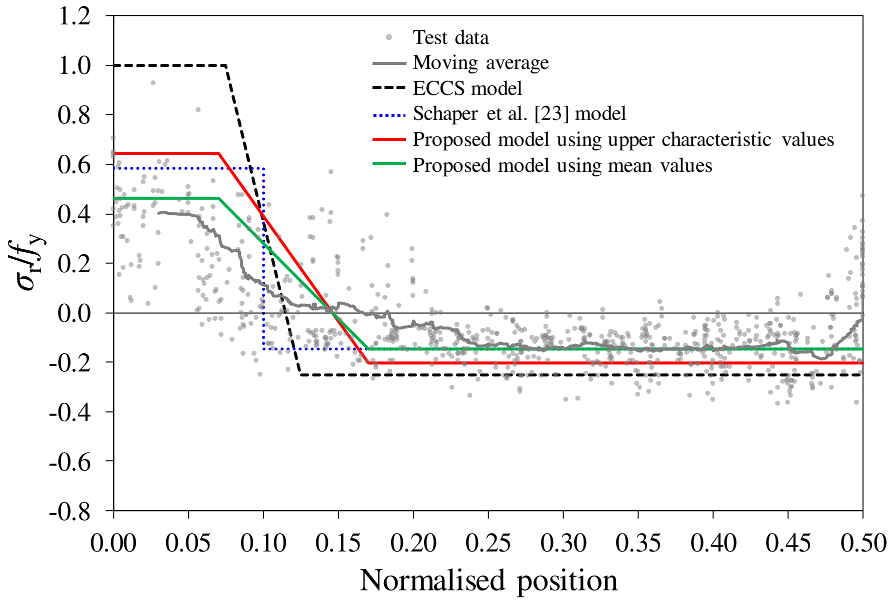

(c) 690 steel welded I-sections

Fig. 1. Comparisons between measured residual stress data and different predictive models

The general residual stress pattern adopted in the two existing models, i.e. the ECCS and the Schaper et al. [23] models, is illustrated in Fig. 2, with the key parameters listed in Table 2, where $\sigma_{r,wt}$ and $\sigma_{r,ft}$ are the maximum tensile residual stresses in the web and the flanges, respectively, $\sigma_{r,wc}$ and $\sigma_{r,fc}$ are the maximum compressive residual stresses in the web and the flanges, respectively, and *a*, *b*, *c* and *d* are stress distribution parameters. It should be noted that the predictive model proposed by Schaper et al. [23] does not feature a linear transition from the compressive to tensile residual stress regions (i.e. the distribution parameters a and d are equal to 0), leading to a stepwise residual stress distribution. It can be seen from Figs. 1(a)-(c) that the ECCS model generally overestimates the residual stress amplitudes and fails to accurately capture the transitional region from tension to compression, particularly for welded I-sections made of the higher steel grades. The residual stress model proposed by Schaper et al. [23] is shown to be capable of accurately capturing the trend of the reducing relative residual stress amplitudes with increasing steel grades; the model does not however represent the presence of the transition regions.

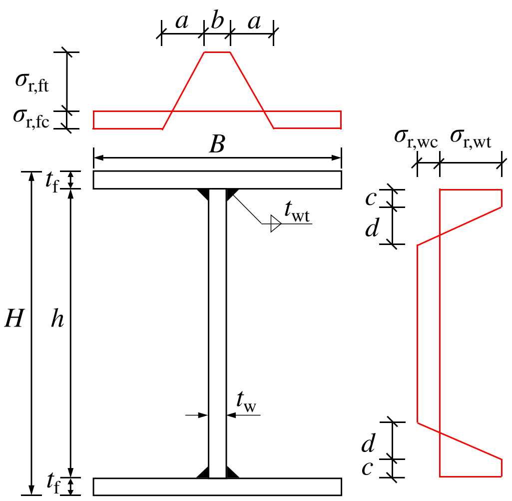

Fig. 2. Proposed residual stress model

Table 2. Parameters employed in different residual stress models

	$\sigma_{r,wt} = \sigma_{r,ft}$	$\sigma_{r,wc} = \sigma_{r,fc}$	a	b	c	d
ECCS [36,37]	f_y	$-0.25f_y$	$0.05B$	$0.15B$	$0.075h$	$0.05h$
Schaper et al. [23]	$f_y\varepsilon^*$	From	0	$\min\{t_w+5t_{wt}^{**},B/5\}$	$0.1h$	0
Proposed model	Eq. (1) or Eq.	From	$0.1B$	$0.14B$	$0.07h$	$0.1h$

$^*\varepsilon=(235/f_y)^{0.5}$, where f_y is the yield strength of the corresponding plate; $^{**}t_{wt}$ is the weld throat thickness, as defined in Fig. 2.

Based on the comprehensive assembled collection of experimental data, believed to be the largest gathered to date, a new residual stress model is proposed herein. The proposed residual stress model adopts the general pattern of the conventional ECCS model, but the key parameters have been re-calibrated against the extensive experimental data, as summarised in Table 2. Compared to the ECCS model, the width of the peak tensile residual regions (i.e. the parameters *b* and *c* for the flanges and web respectively) in the proposed model has been marginally reduced, while the width of the linear transition regions (i.e. the parameters *a* and *b* for the flanges and web respectively) has been extended from 0.05*B* to 0.1*B*. The maximum tensile residual stresses ($\sigma_{r,wt}$ and $\sigma_{r,ft}$) can be determined from Eq. (1) or Eq. (2), which correspond approximately to the mean or upper characteristic (i.e. 95 percentile) values from the analysed experimental database, as indicated in Figs. 3 (a) and (b), respectively. It should be noted that for each of the investigated steel grades, the measured maximum tensile residual stress data were found to follow an approximately normal distribution, with all statistical information obtained by means of the probabilistic modelling approach outlined in [38,39]. Also note that tensile residual stresses exist at the flange tips of welded I-sections fabricated from flame-cut steel plates, but these were, conservatively, not considered in the present proposals, to ensure the general applicability of the model. The maximum compressive residual stresses ($\sigma_{r,wc}$ and $\sigma_{r,fc}$) can then be derived based on self-equilibrium upon determination of the maximum tensile residual stresses. The proposed residual stress models with the mean and upper characteristic maximum tensile residual stresses (determined by Eq. (1) and Eq. (2), respectively) are also plotted in Figs. 1(a)-(c), which are shown to generally agree better with the distributions of the experimental data in comparison with the existing models.

$$\frac{\sigma_{r,wt}\left(\sigma_{r,ft}\right)}{f_y} = -0.5\times\sqrt{\frac{f_y}{235}}+1.32\leq 1 \quad (1)$$

$$\frac{\sigma_{r,wt}\left(\sigma_{r,ft}\right)}{f_y} = -0.5\times\sqrt{\frac{f_y}{235}}+1.5\leq 1 \quad (2)$$

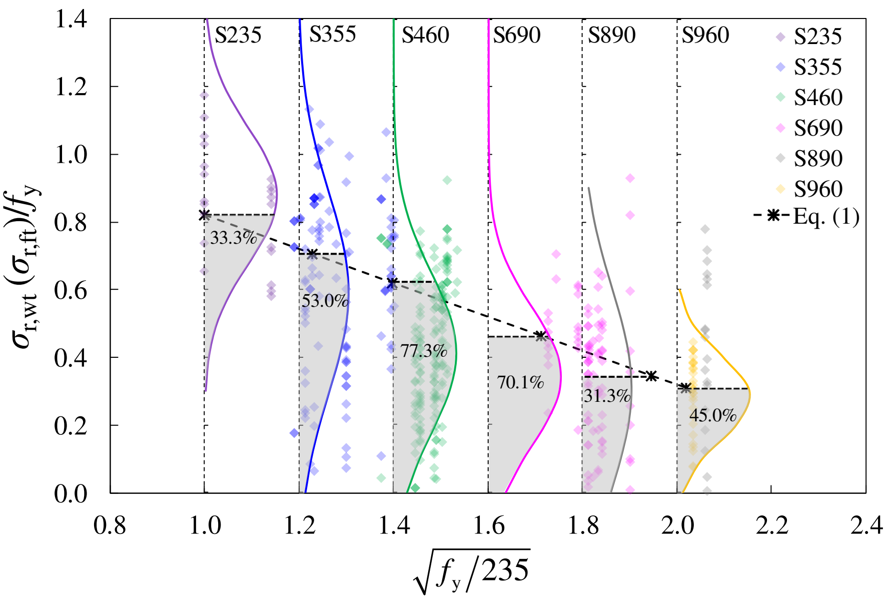

(a) Statistical evaluation of Eq. (1)

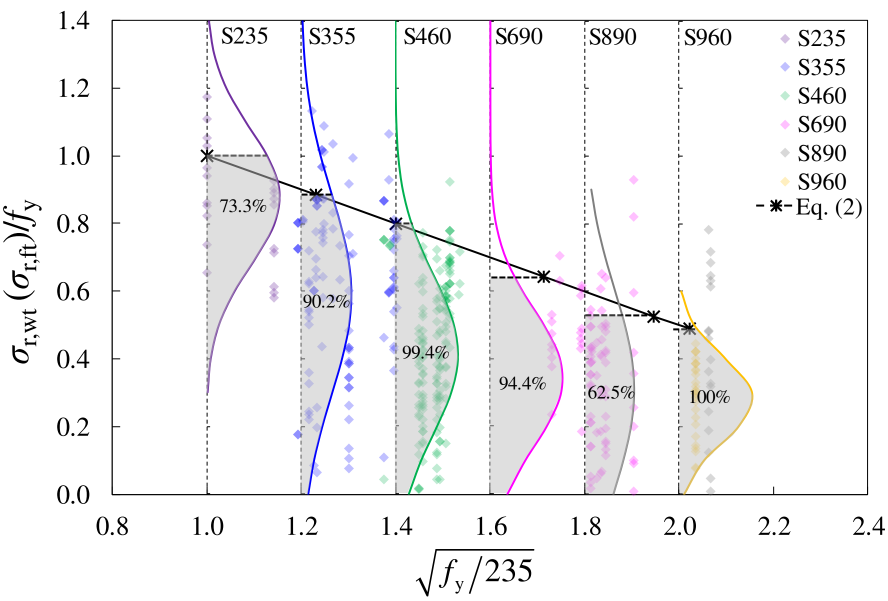

(b) Statistical evaluation of Eq. (2)

Fig. 3. Comparisons between the measured residual stresses within peak tensile residual stress regions and the (a) mean and (b) upper characteristic (95 percentile) maximum tensile residual stresses predicted by Eqs. (1) and (2) respectively, together with statistical distribution diagrams for each of the investigated steel grades.

For doubly symmetric hybrid welded I-sections, the maximum tensile residual stresses in the web $\sigma_{r,wt}$ and the flanges $\sigma_{r,ft}$ should also be determined using Eq. (1) or Eq. (2), but with the value of f_y taken as the greater yield strength of the constituent plates. In cases where the predicted value of the maximum tensile residual stress exceeds the yield strength of the corresponding plate, the maximum tensile residual stress should be taken equal to the yield strength of that plate. As noted in the introduction, it is recommended that Eq. (1) is used in the validation of FE models, while Eq. (2) is used for FE parametric studies and design by advanced analysis [40-42]. This is consistent with the approach typically taken for the treatment of initial geometric imperfections.

3. Experimental investigation

3.1. General

An experimental programme was carried out to address the sparsity of test data on the major axis flexural buckling behaviour of HSS homogeneous and hybrid welded I-section columns. Three welded I-section profiles were investigated in the experimental programme: two homogeneous S690 welded I-sections − I-65×116×8×8 (flange width B × height H × flange thickness t_f × web thickness t_w in mm, labelled "HSS-I1") and I-80×136×8×8 (labelled "HSS-I2"), and a hybrid welded I-section I-80×136×8×8 (labelled "HYB-I3"). The two homogeneous S690 welded I-sections were fabricated from 8 mm-thick quenched and tempered (QT) S690 steel plates, while the hybrid welded I-section comprised flanges fabricated from QT S690 steel plates and a web fabricated from an 8 mm-thick hot-rolled S355 steel plate; the chemical composition of the employed S690 and S355 steels, as listed in the mill certificates, are provided in Table 3. All three investigated welded I-sections were fabricated by means of gas metal arc welding (GMAW) to produce fillet welds with a nominal weld leg length t_{weld} of 5.6 mm. The geometrical configuration and adopted notation for the welded I-sections are shown in Fig. 4. A total of five welded I-section column specimens were fabricated, including one for each of the three investigated profiles and two repeated test specimens. The identifier for each column specimen (e.g. HSS-I1-C-R) consisted of the cross-section label (i.e. HSS-I1, HSS-I2 or HYB-I3), the letter "C" to denote a column and the letter "R" to denote a repeat test. The experimental programme included tensile coupon tests, initial global geometric imperfection measurements and major axis flexural buckling tests, as detailed in the following subsections.

Table 3. Chemical composition for 8 mm-thick S355 and S690 parent plates

Steel grade	C %	Si %	Mn %	P %	S %	N %	Cu %	Mo %	Ni %	Cr %	V %	Nb %	Ti %	B %	Zr %	Al %
S355	0.165	0.475	1.548	0.013	0.0008	-	0.023	0.01	0.029	0.031	0.001	-	-	-	-	0.042
S690	0.139	0.284	1.436	0.013	0.0007	0.0029	0.026	0.068	0.029	0.323	0.002	0.022	0.011	0.0016	0.0002	0.031

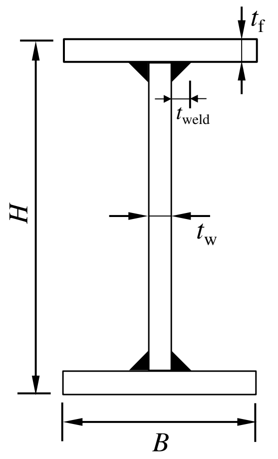

Fig. 4. Geometrical configuration and adopted notation for welded I-sections

3.2. Tensile coupon tests

Tensile coupon tests were carried out to acquire the key material properties and full-range stress-strain curves of the studied S690 and S355 steels. Details regarding the dimensions of the tensile coupons as well as the coupon test setup and loading procedures were reported by the authors in [43], while the key results are briefly summarised in this subsection. The tensile coupons were cut in the longitudinal (rolling) direction and their dimensions are shown in Fig. 5(a). For the two investigated steel grades, two tensile coupons were extracted from each 8 mm-thick parent steel plate along the rolling direction which coincided with the longitudinal direction of the column specimens. The measured engineering stress-strain curves for the two examined steel grades are shown in Fig. 5(b). The average measured values of the key material properties, including the Young's modulus E, the yield strength f_y, the ultimate strength f_u, the strain hardening strain ε_{sh} where the yield plateau ends and subsequently the strain hardening initiates [44], the strain at the ultimate strength ε_u and the fracture strain ε_f measured over a gauge length of 140 mm, are summarised in Table 4. The ultimate-to-yield strength ratio f_u/f_y and strain ratio $\varepsilon_u/\varepsilon_y$ (where $\varepsilon_y = f_y/E$) are also given in Table 4, which are shown to satisfy the material ductility requirements specified in EN 1993-1-1 [12] and EN 1993-1-12 [13] for NSS and HSS, respectively.

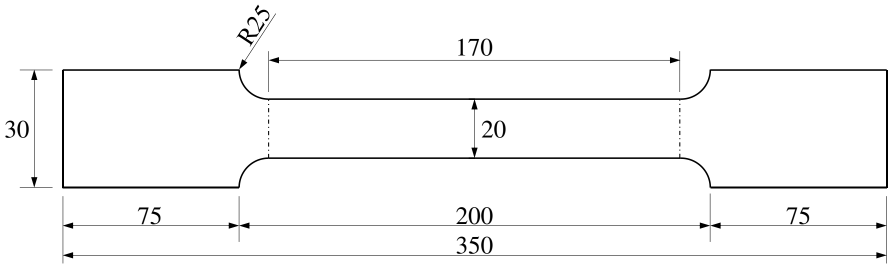

(a) tensile coupon dimension (in mm)

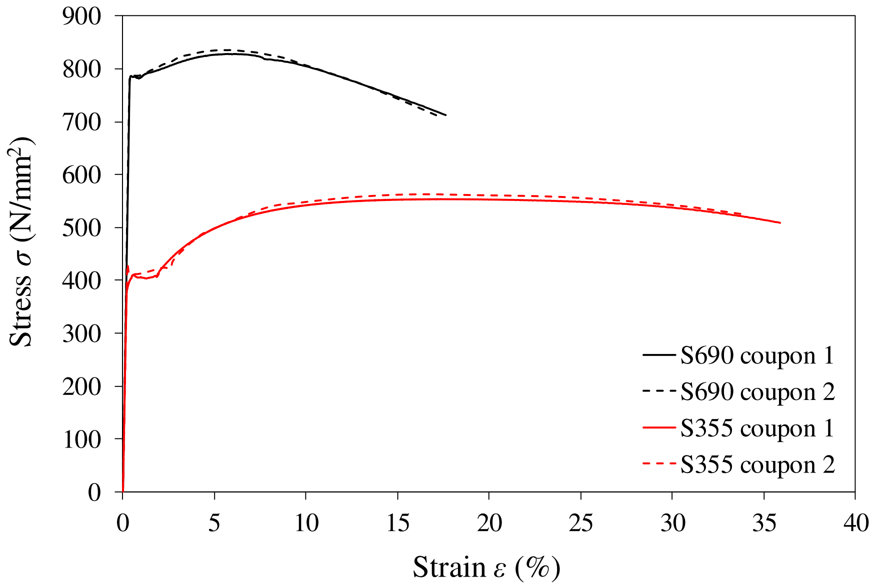

(b) Measured full-range stress-strain curves

Fig. 5. Tensile coupon tests conducted for the present study.

Table 4. Average measured material properties for S355 and S690 steels from tensile coupon tests

Steel grade	E	f_y	f_u	ε_y	ε_{sh}	ε_u	ε_f	f_u/f_y	$\varepsilon_u/\varepsilon_y$
	N/mm^2	N/mm^2	N/mm^2	%	%	%	%	-	-
S355	198500	404.1	553.5	0.20	1.89	17.22	44.8	1.37	84.6
S690	212000	782.5	828.4	0.37	0.96	6.17	19.3	1.06	16.7

3.3. Imperfection measurements

Measurements were taken of initial major axis global geometric imperfections (i.e. out-of-straightness in the direction of buckling) for all five column specimens prior to testing. The test setup for the measurement of the initial global geometric imperfections is shown in Fig. 6, in which the column specimens were clamped to a horizontal bed and two pairs of LVDTs were secured to a trolley that could move up and down a straight aluminium track along the length of the specimens. The same test setup was also successfully employed in [45,46]. The LVDTs were utilised to record the variation in the out-of-straightness along the flange tips over the full column length. The amplitude of the initial global geometric imperfections w_g was taken as the maximum value of the deviations of the recorded displacement readings from a reference datum that passes through the displacement readings recorded at the member ends, as illustrated by the blue dashed line in Fig. 6. The measured imperfection amplitudes w_g are reported in Table 5; all were less than the value of $L_{cr}/1000$, where L_{cr} is the critical effective buckling length of the column specimens between the knife edges.

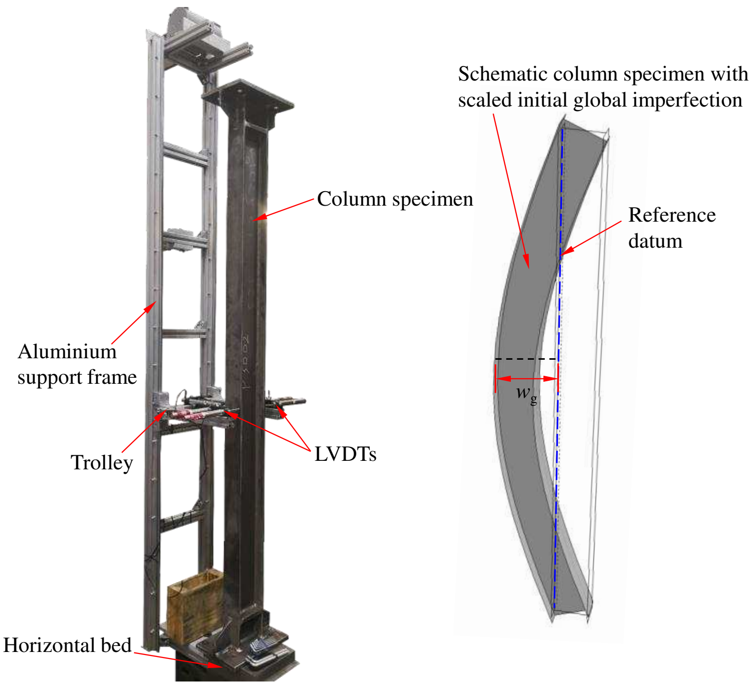

Fig. 6. Test setup for measurement of initial global geometric imperfections and definition of w_g

Table 5. Average measured geometric properties and key results from column buckling tests

Specimen	B mm	H mm	t_f mm	t_w mm	t_{weld} mm	L mm	L_{cr} mm	A mm^2	$\bar{\lambda}$	w_g mm	e_g mm	N_u kN	δ_u mm
HSS-I1-C	65.04	116.77	8.36	8.42	7.08	2000	2182	2028.6	0.94	0.85	2.38	1158.2	6.9
HSS-I1-C-R	65.12	116.60	8.36	8.33	6.71	2000	2182	2010.4	0.94	0.77	2.21	1079.2	5.3
HSS-I2-C	79.58	137.24	8.36	8.26	5.10	2000	2182	2378.3	0.78	1.10	2.40	1418.1	6.0
HYB-I3-C	79.97	136.06	8.32	8.16	7.09	2000	2182	2407.9	0.71	1.08	2.19	1242.5	6.8
HYB-I3-C-R	79.87	136.68	8.37	8.17	6.15	2000	2182	2394.8	0.70	0.92	2.26	1243.5	5.8

3.4. Major axis flexural buckling tests

A total of five pin-ended major axis flexural buckling tests on homogeneous and hybrid welded I-section columns were conducted. The average measured geometric properties for the five column specimens are reported in Table 5. The nominal length L of all column specimens was 2000 mm and two 16 mm-thick end plates were welded onto both ends of the specimens. Stiffeners were also welded at each end of the column specimens to replicate the conditions in parallel tests on structural frames [43], though the stiffeners would be expected to have negligible influence on the column buckling behaviour, as shown in Fig. 7.

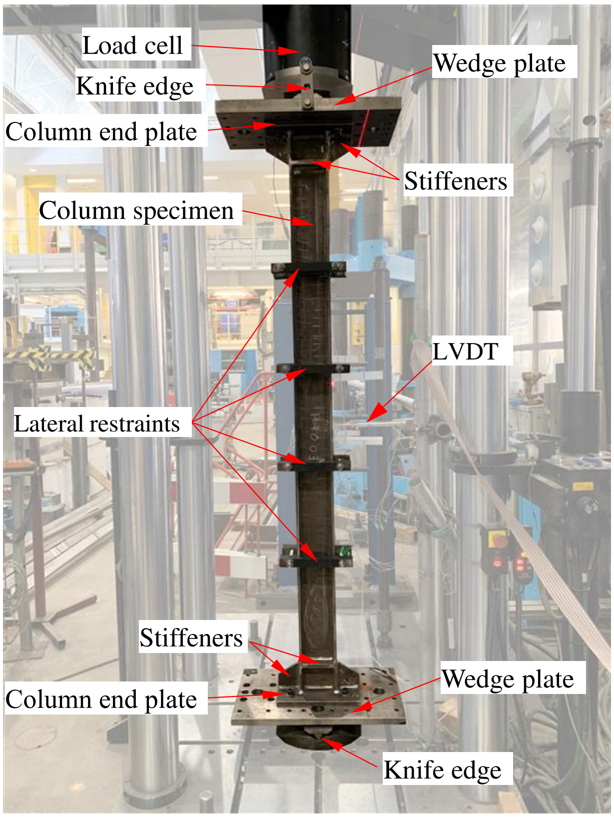

(a) Photograph

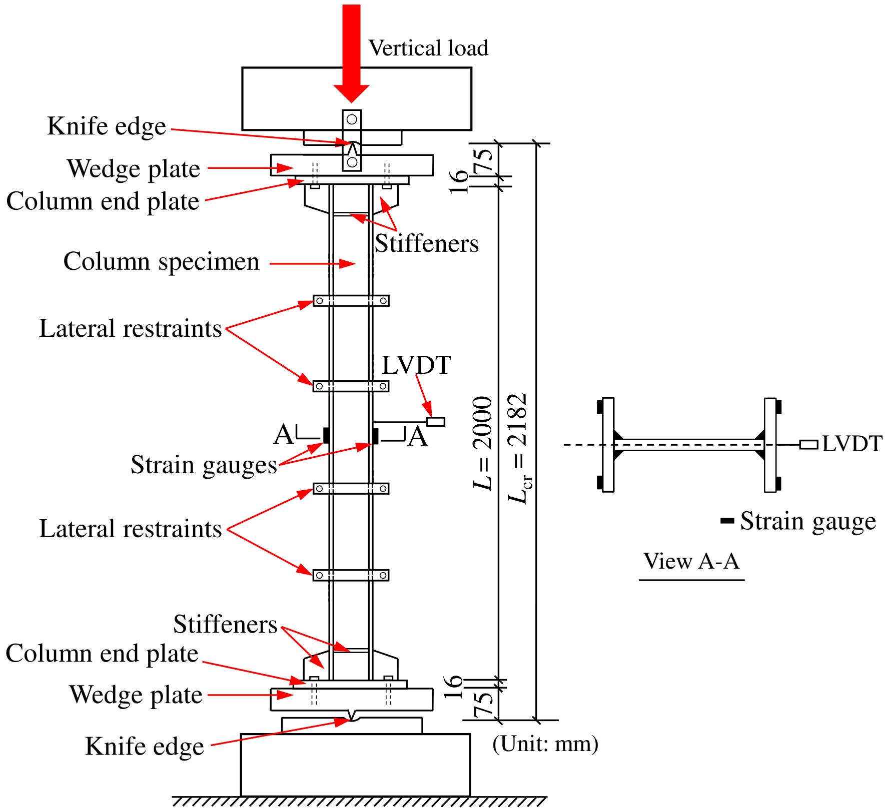

(b) Schematic setup and arrangement of strain gauges and LVDT

Fig. 7. Test setup for pin-ended major axis flexural buckling tests

The column specimens were bolted to the top and bottom wedge plates, and the pin-ended boundary conditions were achieved by means of a pair of knife edges located at a distance of 75 mm from the corresponding column end plate, as illustrated in Fig. 7. The knife edges allowed the column specimens to rotate freely around their major axis but rotation was fixed around the minor axis, leading to an critical effective length L_{cr} for major axis flexural buckling equal to 2182 mm (i.e. the sum of the column specimen length, two column end plate thicknesses and two distances between the knife edge and the corresponding column end plate) for each column specimen. The critical effective length L_{cr} was used in the determination of the non-dimensional member slenderness $\bar{\lambda}$, as defined by Eq. (3) for members with non-slender cross-sections (as was the case for all specimens tested herein), where $N_{c,R}$ is the cross-sectional compression resistance and N_{cr} is the elastic (Euler) buckling load.

$$\bar{\lambda} = \sqrt{\frac{N_{c,R}}{N_{cr}}} = \sqrt{\frac{Af_y}{N_{cr}}} \tag{3}$$

For the hybrid welded I-section columns, the weighted average yield strength $f_{y,a}$ was employed for determining $N_{c,R}$ throughout the present study, as given by Eq. (4), where $f_{y,f}$ and $f_{y,w}$ are the yield strengths of the flange plates and the web plate, respectively, A_f and A_w are the total areas of the flange plates and the web plate, respectively, and A is the cross-sectional area. The non-dimensional member slenderness $\bar{\lambda}$ for each column specimen is provided in Table 5.

$$f_{y,a} = \frac{f_{y,f}A_f + f_{y,w}A_w}{A} \tag{4}$$

All column flexural buckling tests were carried out using an Instron 2000 kN capacity testing machine. For each of the column specimens, four strain gauges were mounted at positions adjacent to the flange tips (at a distance of approximately 5 mm from the tip edges) at mid-height, with a pair of strain gauges on each flange face as illustrated in Fig. 7, to measure the outer fibre strain histories at the critical section. A linear variable displacement transducer (LVDT) was attached at the mid-height of each column specimen, as shown in Fig. 7, for the measurement of the mid-height lateral defections. The initial loading eccentricity e_0 of each column test could be slightly adjusted within the 2 mm clearance between the bolt shanks and the holes in the wedge plates. For each column test, e_0 was adjusted such that the amplitude of the total column global imperfection e_g, equal to the measured initial global geometric imperfections w_g plus the initial loading eccentricity e_0, reached a value as close as possible to L_{cr}/1000, which is conventionally assumed in the development of column buckling design curves [16,17,47]. The adjustment procedure was performed as follows: (1) prior to the actual testing, each column specimen was preloaded to approximately 20% of its expected failure load and the preload outputs, including the applied load and the strain gauge and LVDT readings, were recorded; (2) the present column global imperfection e_g was then determined using Eq. (5), where I is the second moment of area of the welded I-section about its major axis, ε_{max} and ε_{min} are the average strains obtained from the strain gauges on the concave and convex flanges of each column specimen (see Fig. 7), respectively, and N and Δ are the applied axial load and the corresponding mid-height lateral defection measured by the LVDT, respectively; (3) the column position was then carefully adjusted and the above process repeated until the total column global imperfection e_g reached a value sufficiently close to L_{cr}/1000. The same approach to the positioning of column test specimens has been successfully employed in [16,48]. The final values of e_g for all column specimens are provided in Table 5.

$$e_g = \frac{EI\left(\varepsilon_{max} - \varepsilon_{min}\right)}{HN} - \Delta \tag{5}$$

A bespoke restraint system was designed to prevent minor axis buckling of the column specimens without inducing any undesirable influence on their major axis flexural buckling behaviour. The restraint system was composed of a reaction frame and four lateral restraints, as shown in Fig. 8. Each lateral restraint comprised two tee-shaped plates that were placed on either side of the web of the column specimens to clamp the corresponding section by means of two M30 bolts, and a bracing member comprising two parallel square hollow section (SHS) tubes made of S460 steel, as shown in Fig. 9. The assembled tee-shaped plates were connected to the bracing member using an M24 bolt. The shank of the M24 bolt was greased so that the assembled tee-shaped plates would be able to rotate around the bolt shank. Two Macalloy bars with 35 mm diameters, as shown in Fig. 9, were used in each lateral restraint; one allowed adjustment of the length of the bracing member as well as the rotation of the lateral restraint about the axis of the bar, while the other permitted horizontal movement of the lateral restraint in the direction of buckling.

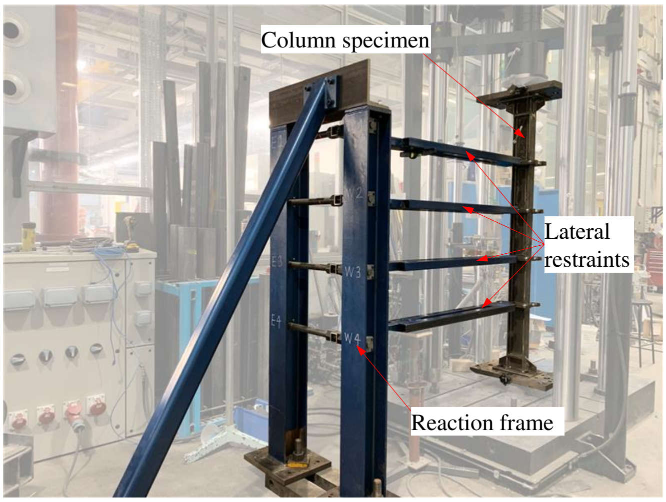

Fig. 8. Restraint system for major axis flexural buckling tests

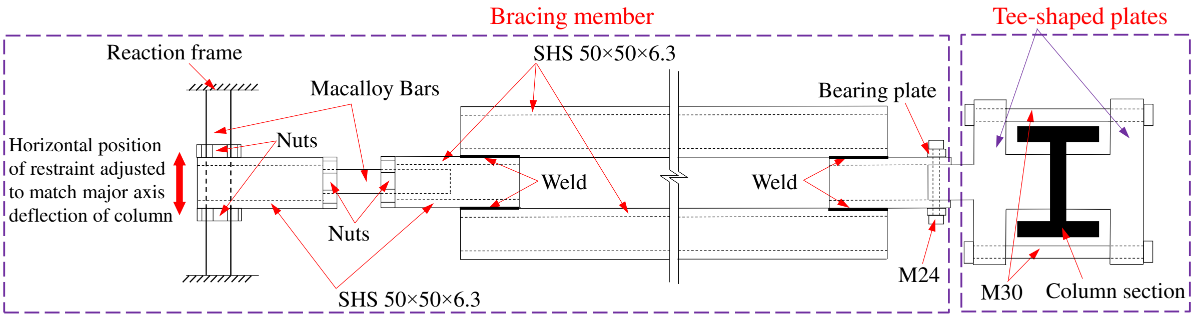

Fig. 9. Schematic drawing of lateral restraint system used in flexural buckling tests

During testing, the horizontal positions of the lateral restraints were continuously adjusted by means of a ratchet spanner to match the lateral deflections of the column specimens at the corresponding heights, as shown in Fig. 10(a). To ensure alignment of the lateral restraints and the column specimens throughout the tests, a pair of rulers with multiple coloured lines at intervals of 2 mm were affixed to both ends of each lateral restraint to serve as a reference for the adjustments; the horizontal positions of the lateral restraints were adjusted according to a laser line projected vertically onto the colour coded rulers, as shown in Fig. 10(b).

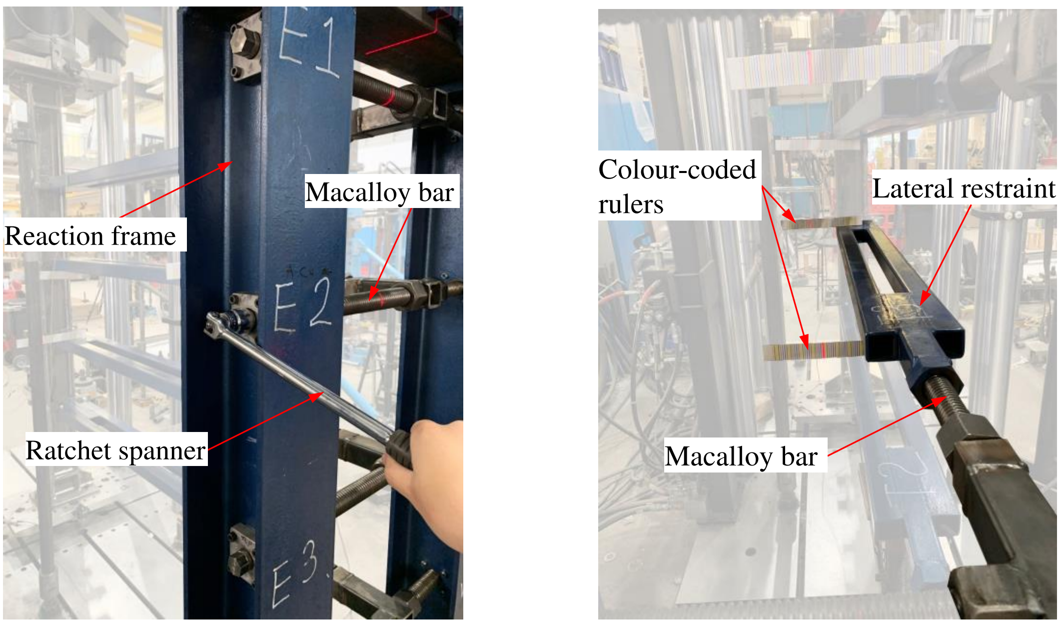

(a) Adjusting horizontal position of lateral restraints using a ratchet spanner

(b) Laser line projected onto colour coded rulers

Fig. 10. Adjustment of horizontal position of lateral restraints during testing

The experimental axial load–mid-height lateral deflection (N-Δ) curves for the homogeneous and hybrid welded I-section columns are presented in Figs. 11(a) and 11(b), respectively. The ultimate major axis flexural buckling load N_u and the corresponding mid-height lateral deflection δ_u for each column specimen are summarised in Table 5. The failure modes of all tested columns are shown in Fig. 12; all column specimens buckled in the direction dictated by the global imperfections. As shown in Fig. 12, the failure of all column specimens was dominated by global buckling with no pronounced local buckling due to the compact nature of the chosen cross-section profiles.

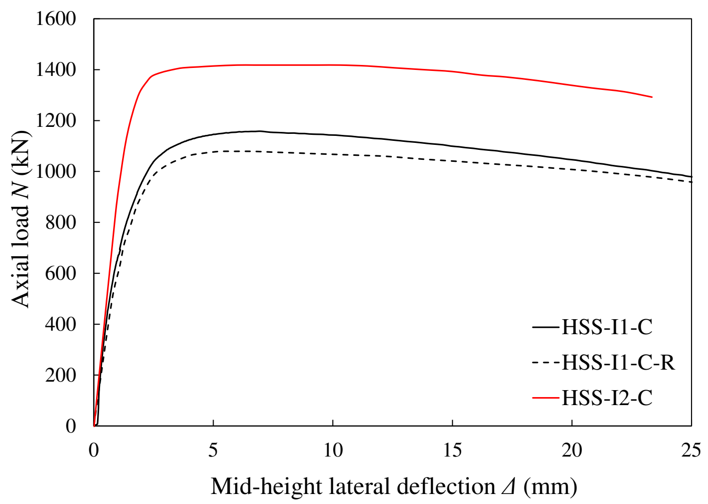

(a) Homogeneous welded I-section columns

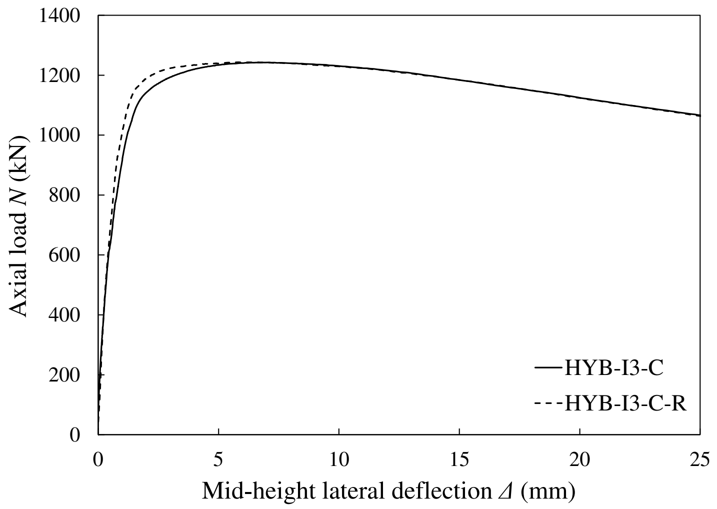

(b) Hybrid welded I-section columns

Fig. 11. Experimental axial load–mid-height lateral deflection curves

HSS-I1-C HSS-I1-C-R HSS-I2-C HYB-I3-C HYB-I3-C-R

Fig. 12. Failure modes of tested welded I-section columns

4. Numerical simulations

4.1. General

In conjunction with the experimental efforts, numerical investigations were performed with the aims of developing reliable finite element (FE) models to replicate the test results and then carrying out comprehensive parametric studies to generate supplementary flexural buckling resistance data for both homogeneous and hybrid welded I-section columns covering a wide range of cross-section dimensions, member slenderness and material grades. Details of the numerical investigations are provided in the present section.

4.2. Development of FE models

The numerical simulations for the welded I-section columns were conducted using the general-purpose FE package Abaqus [49]. All the developed FE models in the present study were meshed with the S4R element (i.e. a four-noded shell element with reduced integration from the Abaqus element library [49]), which has been successfully applied in previous numerical investigations of I-section structural components subjected to different loading conditions [3,50-[54]. For validation purposes, the measured cross-sectional geometries of welded I-sections including the weld fillets were carefully modelled. The weld fillets were assumed to be symmetric and represented by five web elements with equal height but different widths (i.e. thicknesses), as illustrated in Fig. 13. In order to avoid any overlap between the flange and web plates, nodes at both edges of the web were offset from the web-to-flange junctions by half the flange thickness, and coupled to their corresponding nodes at the mid-thickness of the flange plates using *MPC BEAM constraints, as depicted in Fig. 13.

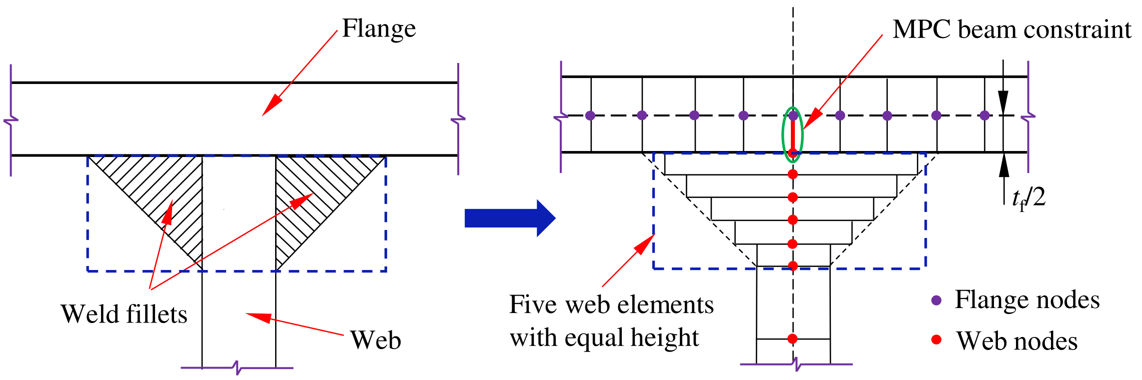

Fig. 13. Modelling technique for geometrical representation of weld fillets in welded I-sections

Following a mesh sensitivity investigation, an element size approximately equal to $(B+H)/40$ was selected to discretise the modelled column specimens in both the transverse and longitudinal directions; the adopted mesh density was shown to provide sufficiently accurate results with reasonable computational efficiency. The measured engineering stress-strain curves were transformed into true stress-logarithmic plastic strain curves before input into Abaqus.

Both initial local and global geometric imperfections were introduced into the FE models by modifying the nodal coordinates of the original perfect geometry. Local geometric imperfections were included in the form of a series of sinusoidal waves (see Fig. 14) with their half-wavelength approximately equal to the elastic local buckling half-wavelength of the modelled welded I-section in compression $L_{b,cs}$, which can be determined numerically (e.g.

using the readily available finite strip software CUFSM [55]) or approximated using analytical expressions developed by Fieber et al. [56]; the former was employed herein. The local imperfection amplitude of the web δ_{w} was taken as 1/200 of the web height h_{w} (i.e. $h_{\mathrm{w}} = H - 2t_{\mathrm{f}} - 2t_{\mathrm{weld}}$) when the web plate was more susceptible to local buckling than the flange plates (i.e. when the web plate had a higher plate slenderness $\bar{\lambda}_{\mathrm{p,w}}$ than that of the flange plates $\bar{\lambda}_{\mathrm{p,f}}$ determined in accordance with EN 1993-1-5 [57]), otherwise the local imperfection amplitude of the flange δ_{f} was taken as 1/50 of the clear width of the flange outstand b_{f} (i.e. $b_{\mathrm{f}} = (B - t_{\mathrm{w}})/2 - t_{\mathrm{weld}}$). The flange plate slenderness $\bar{\lambda}_{\mathrm{p,f}}$ and web plate slenderness $\bar{\lambda}_{\mathrm{p,w}}$ were determined from Eqs. (6) and (7), respectively:

$$\bar{\lambda}_{\mathrm{p,f}} = \sqrt{\frac{f_{\mathrm{y,f}}}{\sigma_{\mathrm{cr,f}}}} = \frac{b_{\mathrm{f}} / t_{\mathrm{f}}}{28.4\varepsilon_{\mathrm{f}}\sqrt{k_{\sigma}}} \tag{6}$$

$$\bar{\lambda}_{\mathrm{p,w}} = \sqrt{\frac{f_{\mathrm{y,w}}}{\sigma_{\mathrm{cr,w}}}} = \frac{h_{\mathrm{w}} / t_{\mathrm{w}}}{28.4\varepsilon_{\mathrm{w}}\sqrt{k_{\sigma}}} \tag{7}$$

in which $\sigma_{\mathrm{cr,f}}$ and $\sigma_{\mathrm{cr,w}}$ are the elastic local buckling stresses of the isolated flange and web plates, respectively, assuming simply-supported boundary conditions at the edges of the adjoining plates, $\varepsilon_{\mathrm{f}} = \sqrt{235 / f_{\mathrm{y,f}}}$ and $\varepsilon_{\mathrm{w}} = \sqrt{235 / f_{\mathrm{y,w}}}$ are the flange and web material parameters, respectively, and k_{σ} is the elastic buckling factor that is equal to 0.43 for the isolated outstand flange under uniform compression and 4 for the isolated internal web under uniform compression, respectively, in accordance with EN 1993-1-5 [57]. Once the local imperfection amplitude of the critical plate was known, the corresponding amplitude for the non-critical plate was determined based on the assumption that the angle of the web-to-flange junctions remained at 90°. The adopted local imperfection amplitudes correspond to the fabrication tolerances for welded I-section members according to EN 1090-2 [58].

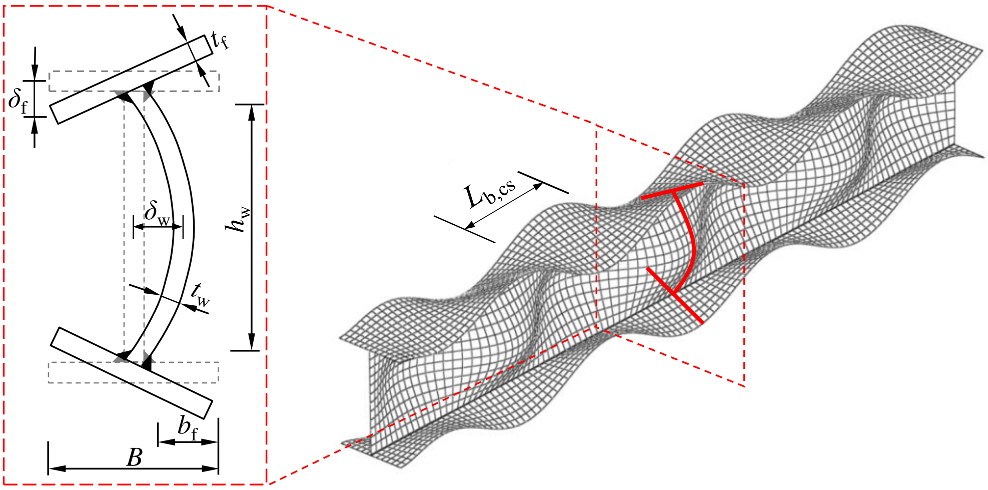

Fig. 14. Form of local geometric imperfections (not to scale) employed in FE models

Global geometric imperfections about the buckling axis were assigned to the FE models in the shape of a half-sine wave along the longitudinal direction of the column. A total of four global imperfection amplitudes, namely the measured global imperfection e_g and three generalised values of $L_{cr}/1000$, $L_{cr}/1500$ and $L_{cr}/2000$, were considered in order to investigate the sensitivity of the FE models to variations in the global imperfection amplitudes. The Abaqus input files containing the nodal coordinates with the pre-defined local and global imperfections were generated using the software package Matlab [59].

The proposed residual stress pattern for welded I-sections, as described in Section 2 of the present study, was employed in the FE models; the residual stresses were taken to be constant through the thickness (i.e. membrane stresses) and simulated explicitly as an initial stress condition by means of the Abaqus *INITIAL CONDITIONS command. To illustrate the impact of the residual stress amplitudes on the flexural buckling resistances of welded I-section columns, both the mean and upper characteristic values of the residual stresses (denoted as

"RS_m" and "RS_uc", respectively), as determined using Eqs. (1) and (2) respectively, were considered in the FE models.

With regards to the boundary conditions, all nodes at each end section of the column specimens were coupled to a reference point, positioned on the centroid axis of the cross-section at the location of the corresponding knife edge, by means of kinematic coupling constraints. Suitable boundary conditions were then applied to the reference points to simulate the pin-ended boundary conditions. Note that for the simulation of the major axis flexural bucking tests carried out in the present study, the out-of-plane displacement degree of freedom at the web-to-flange junction was also restrained at the cross-sections where the lateral restrains were provided, as shown in Fig. 8, thus eliminating the influence of out-of-plane buckling which is beyond the scope of the present study.

4.3. Validation of FE models

The developed FE models were validated against the experimental results from the minor axis flexural buckling tests on homogeneous welded I-section columns reported in [1,2,4] and the major axis flexural buckling tests on both homogeneous and hybrid welded I-section columns described in Section 3. Table 6 presents the ratios of the ultimate resistances obtained from the physical tests $N_{u,test}$ to the ultimate resistances derived from the FE models $N_{u,FE}$ considering the different combinations of the amplitudes of global geometric imperfections and residual stresses. The statistical mean and COV (i.e. coefficient of variation) values of the $N_{u,test}/N_{u,FE}$ ratios for the column specimens buckling about the major axis and about the minor axis, as well as for all specimens, are presented in Table 6. The results of the comparisons show that the best agreement between the test and FE ultimate resistances was achieved when the combination of the measured global imperfection amplitude and the mean value of the residual stresses (i.e. RS_m) was employed. Using the combination of $L_{cr}/1000$ and RS_m in the FE models also results in overall accurate and consistent predictions of the test ultimate resistances, though the numerical resistance predictions for column specimens buckling about the minor axis were slightly conservative since the global imperfection amplitudes of $L_{cr}/1000$ are generally greater than the measured values [1,2,4]. The experimental axial load–mid-height lateral deflection curves were well replicated by the FE models using the amplitude combination of $L_{cr}/1000$ and RS_m, as shown in Fig. 15 for three representative welded I-section column specimens.

Table 6. Comparisons of welded I-section column test results with FE results for varying combinations of global geometric imperfection and residual stress amplitudes

Reference	Cross-section type (steel grade)	Specimen label	Buckling axis	$N_{u,test}/N_{u,FE}$ (Global geometric imperfection and residual stress combinations)							
				RS_m				RS_uc			
				Measured	$L_{cr}/1000$	$L_{cr}/1500$	$L_{cr}/2000$	Measured	$L_{cr}/1000$	$L_{cr}/1500$	$L_{cr}/2000$
Deng et al. [1]	Homogeneous (Q460GJ)	H36	Minor axis	1.04	1.06	1.05	1.04	1.09	1.11	1.10	1.09
		H43		1.10	1.14	1.12	1.11	1.17	1.21	1.19	1.18
		H50		0.98	1.01	0.98	0.97	1.06	1.08	1.06	1.04
		H57		1.05	1.08	1.04	1.02	1.13	1.16	1.12	1.09
		H64		0.94	1.01	0.96	0.93	1.01	1.07	1.02	1.00
		H72		1.00	1.16	1.09	1.06	1.06	1.22	1.15	1.12
		H78		1.02	1.09	1.03	1.00	1.06	1.14	1.07	1.04
		H86		0.94	1.02	0.97	0.94	0.96	1.06	1.00	0.96
Li et al. [4]	Homogeneous (Q690)	H-30-1		1.07	1.07	1.05	1.05	1.12	1.12	1.11	1.10
		H-30-2		1.08	1.12	1.10	1.09	1.15	1.18	1.16	1.16
		H-50-1		1.08	1.17	1.13	1.10	1.15	1.24	1.20	1.17
		H-50-2		1.07	1.15	1.11	1.09	1.15	1.22	1.18	1.16
		H-70-2		0.88	0.96	0.92	0.89	0.90	0.99	0.94	0.91
Ban et al. [2]	Homogeneous (Q960)	H2-960		1.02	0.95	0.91	0.89	1.04	0.98	0.94	0.91
		H3-960		1.08	1.08	1.06	1.05	1.08	1.08	1.06	1.05
Mean for column specimens buckling about the minor axis				1.02	1.07	1.03	1.02	1.08	1.12	1.09	1.07
COV for column specimens buckling about the minor axis				0.06	0.06	0.07	0.07	0.07	0.07	0.08	0.08
Present study	Hybrid (Q690 + Q355)	HSS-I1-C	Major axis	0.98	0.97	0.94	0.93	1.00	1.03	1.00	0.99
		HSS-I1-C-R		0.94	0.94	0.92	0.90	1.03	1.02	0.98	0.97
		HSS-I2-C		0.95	0.93	0.91	0.90	1.00	0.98	0.96	0.96
		HYB-I3-C		1.00	1.00	0.99	0.98	1.02	1.02	1.03	1.02
		HYB-I3-C-R		1.01	1.00	0.99	0.98	1.03	1.03	1.03	1.02
Mean for column specimens buckling about the major axis				0.98	0.97	0.95	0.94	1.02	1.01	1.00	0.99
COV for column specimens buckling about the major axis				0.03	0.04	0.04	0.04	0.02	0.02	0.03	0.03
Mean for all column specimens				1.01	1.04	1.01	0.99	1.06	1.10	1.06	1.05
COV for all column specimens				0.06	0.07	0.07	0.08	0.07	0.08	0.08	0.08

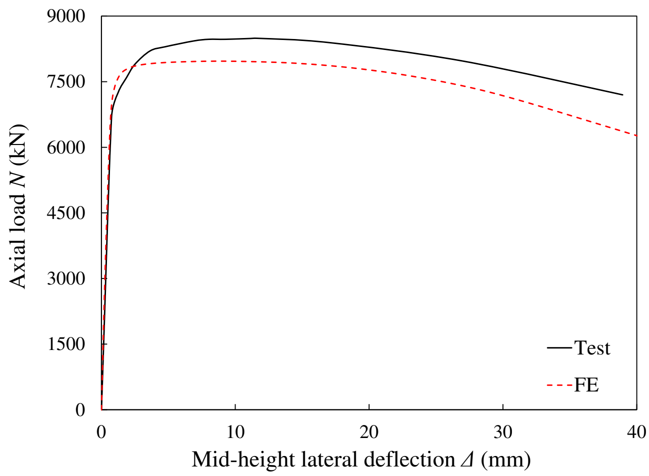

(a) Q690 steel homogeneous welded I-section column buckling about the minor axis (Specimen H-30-1 tested in [4])

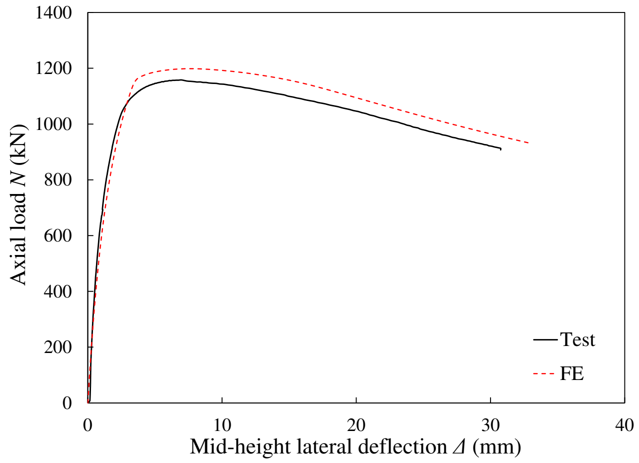

(b) S690 steel homogeneous welded I-section column buckling about the major axis (Specimen HSS-I1-C)

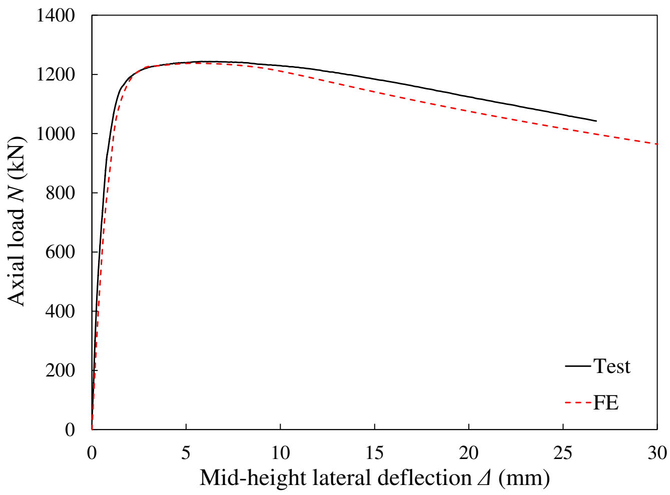

(c) Hybrid welded I-section column buckling about the major axis (Specimen HYB-I3-C)

Fig. 15. Comparisons of typical test and FE load-deformation curves for welded I-section columns

It may be observed from Table 6 that the amplitude of the residual stresses has a clear influence on the ultimate resistances of the welded I-section columns. The increase in residual stress amplitude (i.e. from RS_m to RS_uc) is more detrimental to the welded I-section columns buckling about the minor axis due to the added flange compressive residual stresses promoting earlier yielding at the flange tips, which make the greatest contribution to the member stability. Use of the RS_uc residual stresses in the FE models resulted in an average decrease in capacity of almost 5% in comparison to that obtained from the FE models with the RS_m residual stresses.

To conclude, the developed FE models using the combination of measured (or $L_{cr}/1000$ if measurements are unavailable) geometric imperfection amplitudes and RS_m residual stresses have been shown to be able to accurately simulate the observed behaviour of welded I-section columns and are suitable for FE model validation. For parametric studies, on the other hand, where more safe-sided results are typically sought, use of the combination of $L_{cr}/1000$ geometric imperfection amplitudes and RS_uc residual stresses is recommended.

4.4. Numerical parametric studies

Following the successful validation of the developed FE models, comprehensive numerical parametric studies were performed with the aim of expanding the data pool for both homogeneous and hybrid welded I-section columns over a wider variety of steel grades, cross-sectional geometries and member slendernesses. Five hot-rolled steel grades were considered in the parametric studies: S235, S355, S460, S690 and S960, leading to a total of five different homogeneous welded I-sections and five different hybrid welded I-sections (i.e. I-sections made of (1) S460 steel flanges and an S235 steel web, (2) S460 steel flanges and an S355 steel web, (3) S690 steel flanges and an S355 steel web, (4) S690 steel flanges and an S460 steel web and (5) S960 steel flanges and an S690 steel web) being investigated. The bilinear plus nonlinear hardening material model developed by Yun and Gardner [44] was used to derive the full-range stress-strain curves for the S235, S355, S460 and S690 hot-rolled steels. Owing to the fact that only a limited number of experimental stress-strain curves on ultra-high strength S960 steel were available to underpin the Yun and Gardner model [44], the average measured stress-strain curve obtained from the longitudinal tensile coupon tests on S960 steel reported in [49] was adopted to simulate the S960 steel plates considered herein. The employed full-range stress-strain curves for the five studied steel grades are shown in Fig. 16, and the corresponding basic mechanical properties (E, f_y and f_u) are provided in Table 7. Note that the basic mechanical properties for the S235, S355, S460 and S690 hot-rolled steels are taken in accordance with the latest version of Eurocode 3 (EC3) − prEN 1993-1-1 [14], while the additional material parameters (e.g. ε_{sh} and ε_u) which are used to form the stress-strain curves, were determined from the predictive expressions given in [44].

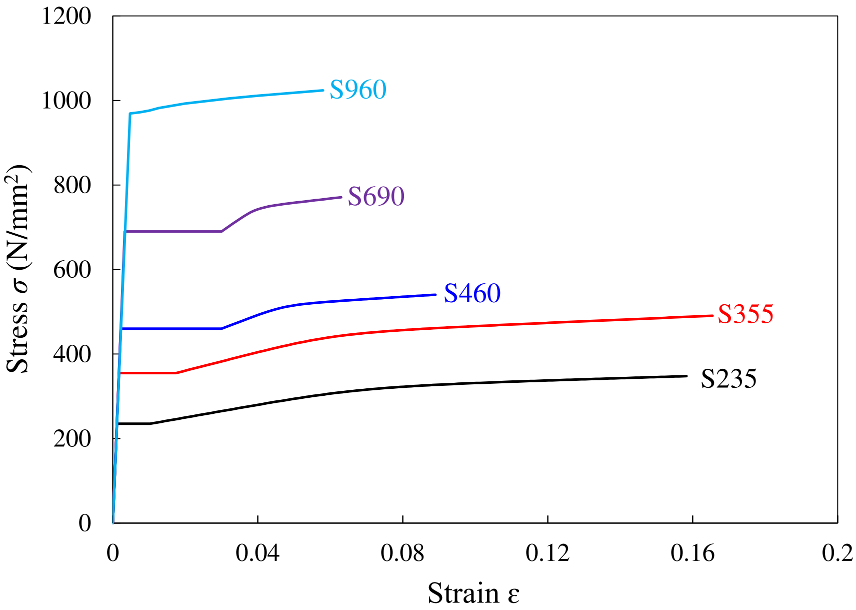

Fig. 16. Full-range stress-strain curves for five hot-rolled steel grades employed in parametric studies

Table 7. Basic mechanical properties for five hot-rolled steel grades employed in parametric studies

Steel grade	E N/mm^2	f_y N/mm^2	f_u N/mm^2
S235	210000	235	360
S355	210000	355	490
S460	210000	460	540
S690	210000	690	770
S960	204393	969	1024

Regarding the welded I-section geometries, a constant flange width B of 100 mm was adopted in the numerical parametric studies, while the cross-section height H was varied to obtain three cross-section aspect ratios H/B of 1.0, 1.5 and 2.0. For each cross-section aspect ratio, five different values of flange thickness t_f (ranging from 5 mm to 20 mm) and web thickness t_w (ranging from 2.8 mm to 28 mm) were employed to generate a broad spectrum of cross-section slendernesses within the Class 1-3 domain according to prEN 1993-1-1 [14]. The t_f and t_w values for all simulated sections were specified such that $\bar{\lambda}_{p,f} \approx \bar{\lambda}_{p,w}$, thus minimising the influence of element interaction between the flanges and web on the local buckling behaviour of the sections [60]. The fillet welds at the web-flange intersections were ignored for all the modelled welded I-section columns in both the parametric studies and, for consistency, the subsequent analysis and assessment/establishment of design provisions. Columns with twenty different lengths were simulated for each cross-section to achieve a broad range of non-dimensional member slenderness $\bar{\lambda}$ from 0.2 to 2.5. The tolerance-based local geometric imperfection amplitudes, together with the amplitude combination of $L_{cr}/1000$ (i.e. the amplitude of global geometric imperfections) and RS_uc (i.e. the amplitude of the residual stresses), were employed throughout the parametric studies. For the column specimens buckling about the major axis, out-of-plane lateral displacements were restrained at the web-flange junction at regular intervals.

A total of 6000 numerical data on homogeneous and hybrid welded I-sections columns were generated, covering flecural buckling about both the major and minor axes, as well as various steel grades, cross-section geometries and member slendernesses. The numerically derived data, together with the available experimental results, are used in the next section for the assessment of existing design provisions and development of new design proposals for both homogeneous and hybrid welded I-section columns.

5. Evaluation of the current design codes and new design proposals

5.1. General

In this section, the applicability and accuracy of the relevant column buckling design provisions, as set out in prEN 1993-1-1 [14] and AISC 360 [15], are assessed for the design of both homogeneous and hybrid welded I-section columns made of varying steel grades. The assessment was made by comparing the ultimate loads obtained from the tests and FE simulations $N_{u,test/FE}$ to the unfactored resistance predictions determined according to prEN 1993-1-1 ($N_{u,EC3}$) or AISC 360 ($N_{u,AISC}$). Shortcomings in the current design rules are revealed; hence, new design proposals to overcome the identified shortcomings are developed.

5.2. European code prEN 1993-1-1 (EC3)

The latest version of prEN 1993-1-1 (EC3) [14] specifies different column buckling curves based on the Ayrton-Perry type formulation [62] for the design of structural steel column members with material grades up to S700 susceptible to global instability (i.e. flexural buckling, torsional buckling and flexural-torsional buckling). The flexural buckling resistance $N_{b,EC3,Rd}$ of welded I-section columns with non-slender cross-sections (i.e. Class 1-3 cross-sections) is given by Eq. (8):

$$N_{\mathrm{b,EC3,Rd}} = \frac{\chi_{\mathrm{EC3}} A f_{\mathrm{y}}}{\gamma_{\mathrm{M1}}}, \text{ for non-slender welded I-section columns} \quad (8)$$

in which γ_{M1} is the partial safety factor for member buckling, with a recommended value of 1.0 [14], and χ_{EC3} is the EC3 flexural buckling reduction factor, as given by Eqs. (9) and (10):

$$\chi_{\mathrm{EC3}} = \frac{1}{\phi_{\mathrm{EC3}} + \sqrt{\phi_{\mathrm{EC3}}^2 - \bar{\lambda}^2}} \text{ but } \chi_{\mathrm{EC3}} \leq 1.0 \quad (9)$$

$$\phi_{\mathrm{EC3}} = 0.5\left(1 + \alpha_{\mathrm{EC3}}\left(\bar{\lambda} - \bar{\lambda}_{0,\mathrm{EC3}}\right) + \bar{\lambda}^2\right) \quad (10)$$

where $\bar{\lambda}$ is the non-dimensional member slenderness given by Eq. (3) and α_{EC3} (i.e. the imperfection factor) and $\bar{\lambda}_{0,\mathrm{EC3}}$ (i.e. the plateau length of the buckling curve) are parameters that account for the combined effects of geometric imperfections and residual stresses on the flexural buckling resistances of column members; the values of α_{EC3} and $\bar{\lambda}_{0,\mathrm{EC3}}$ for different cross-section shapes and design parameters are specified in prEN 1993-1-1 [14]. Specifically, prEN 1993-1-1 [14] adopts buckling curve "c" (with $\bar{\lambda}_{0,\mathrm{EC3}}$ = 0.2 and α_{EC3} = 0.49) for homogeneous welded I-section columns with $t_{\mathrm{f}} \leq 40$ bucking about the minor axis and buckling curve "b" (with $\bar{\lambda}_{0,\mathrm{EC3}}$ = 0.2 and α_{EC3} = 0.34) for homogeneous welded I-section columns with $t_{\mathrm{f}} \leq 40$ bucking about the major axis for all grades of steel.

The accuracy and suitability of the EC3 column buckling curves for both homogeneous and hybrid welded I-section columns made of varying steel grades are assessed based on the established test and FE data. Note that the yield strength f_y is replaced by the weighted average yield strength $f_{y,a}$ given by Eq. (4) for the determination of the non-dimensional member slenderness $\bar{\lambda}$ (using Eq. (3)) and the EC3 flexural buckling resistance (using Eq. (8)) of the hybrid welded I-section columns. The test and FE ultimate resistances $N_{u,test/FE}$ are normalised by the unfactored EC3 resistance predictions $N_{u,EC3}$ and plotted against the column non-dimensional member slenderness $\bar{\lambda}$ (i.e. $\bar{\lambda} = \sqrt{Af_y / N_{cr}}$ for the homogeneous welded I-section columns and $\bar{\lambda} = \sqrt{Af_{y,a} / N_{cr}}$ for the hybrid welded I-section columns) in Fig. 17. It can be seen from Fig. 17 that the EC3 design approach yields flexural buckling resistance predictions with varying levels of accuracy for columns made of different steel grades. The EC3 resistance predictions are generally conservative for welded I-sections columns made of HSS grades (i.e. S690 steel and S960 steel), while a number of EC3 resistance predictions appear on the unsafe side for columns made of NSS grades (i.e. homogeneous welded I-sections made of S235, S355 and S460 steels, and hybrid welded I-sections made of S460 steel flanges and an S235 steel web as well as S460 steel flanges and an S355 steel web) with intermediate to low non-dimensional member slenderness values. The resistance predictions are also rather scattered, which is also evident from the statistical results of the ratios of $N_{u,test/FE}/N_{u,EC3}$ presented in Table 8. The high level of scatter of the EC3 design provisions can be principally attributed to the fact that only a single column buckling curve is employed for the design of welded I-section columns buckling about each axis with different steel grades (i.e. curve “c” for flexural buckling about the minor axis and curve “b” for flexural buckling about the major axis), which fails to capture the trend of the reducing relative influence of imperfections, both residual stresses and global geometric imperfections, on the flexural buckling resistances of columns with increasing steel grades [16,17]. This shortcoming was addressed in a recent research project named Stronger Steels in the Built Environment (STROBE) [61] where higher flexural buckling curves were proposed for welded I-sections made of S460 steel and above (i.e. using curve "b" for flexural buckling about the minor axis and curve "c" for flexural buckling about the major axis). The ratios of the test and FE column flexural buckling resistances to the resistance predictions using the proposed design curves in STROBE $N_{u,test/FE}/N_{u,STROBE}$ are presented in Table 8. It can be seen from Table 8 that the proposed design curves in STROBE yield improved resistance predictions in terms of both accuracy and consistency compared to the existing EC3 design provisions, though with scope for further improvement.

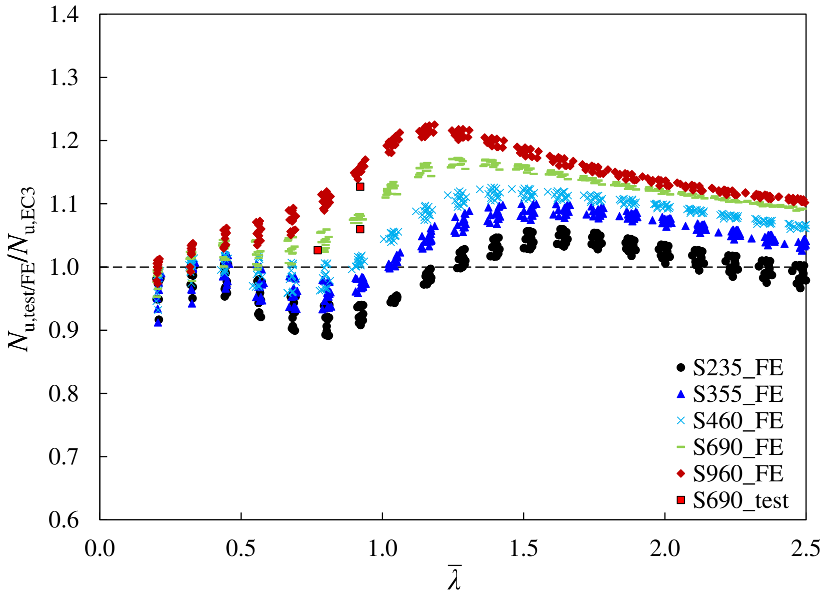

(a) Homogeneous welded I-section columns buckling about the major axis

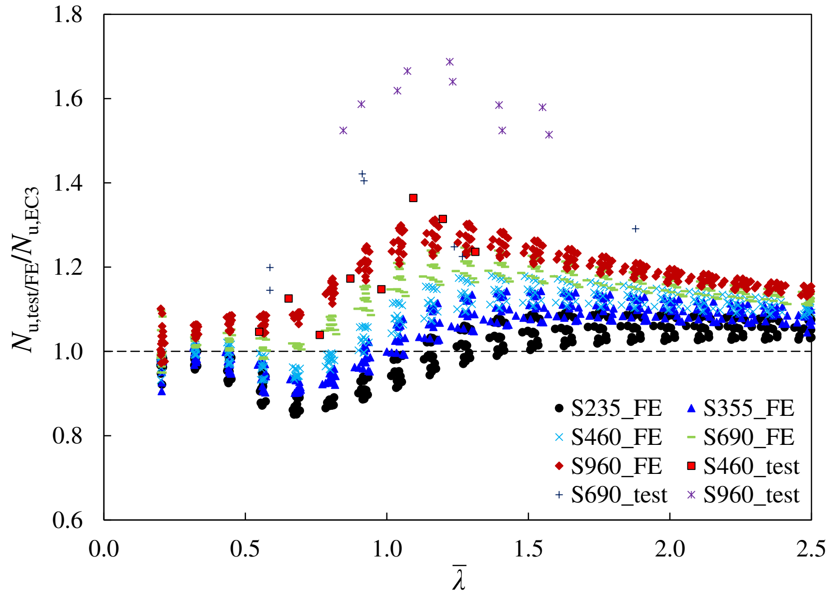

(b) Homogeneous welded I-section columns buckling about the minor axis

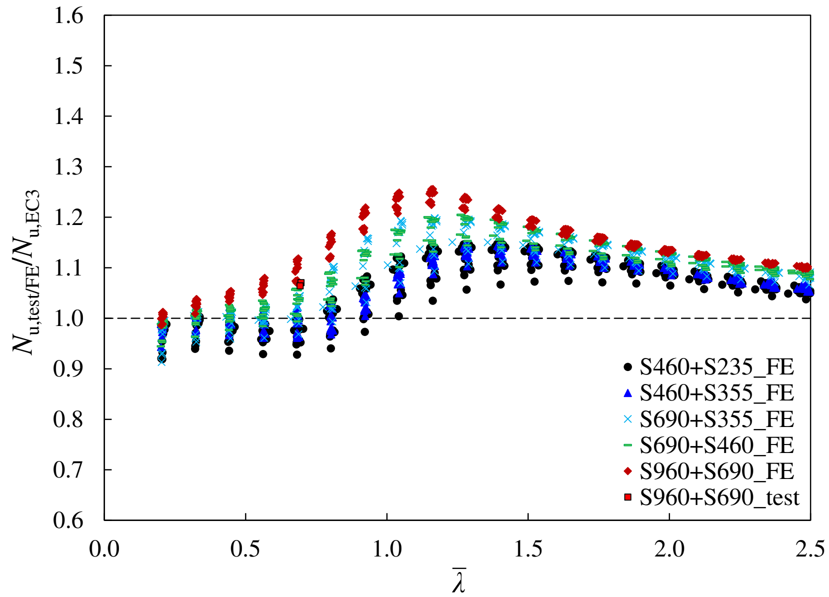

(c) Hybrid welded I-section columns buckling about the major axis

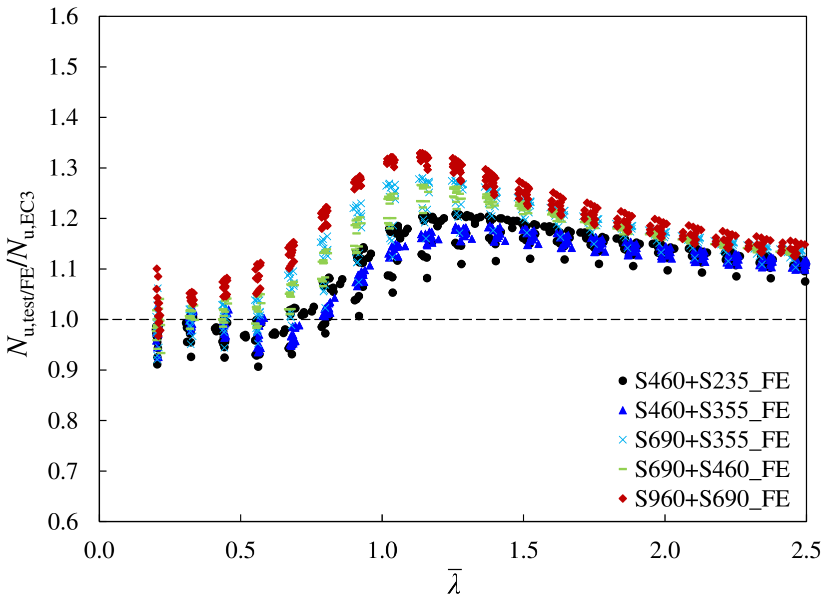

(d) Hybrid welded I-section columns buckling about the major axis

Fig. 17. Comparisons of test and FE ultimate resistances of column specimens with those predicted using prEN 1993-1-1 [14]

Table 8. Comparisons of test and FE ultimate resistances of column specimens with those predicted using different design methods

Column type	Buckling axis	Number of data points FE (test)	Evaluation parameter	prEN 1993-1-1 [14]	STROBE proposal [61]	AISC 360 [15]	Modified EC3
				$N_{u,test/FE}/N_{u,EC3}$	$N_{u,test/FE}/N_{u,STROBE}$	$N_{u,test/FE}/N_{u,AISC}$	$N_{u,test/FE}/N_{u,mod-EC3}$
Homogeneous welded I-section	Major	1500 (3)	Mean	1.061	1.017	0.998	1.071
			COV	0.070	0.049	0.060	0.039
Homogeneous welded I-section	Minor	1500 (35)	Mean	1.088	1.042	0.956	1.062
			COV	0.104	0.079	0.087	0.062
Hybrid welded I-section	Major	1500 (2)	Mean	1.091	1.018	1.026	1.075
			COV	0.069	0.050	0.045	0.047
Hybrid welded I-section	Minor	1500 (0)	Mean	1.132	1.056	0.993	1.089
			COV	0.080	0.065	0.054	0.054

5.3. American specification AISC 360 (AISC)

The American Specification AISC 360 [15] employs the following equation for the determination of the flexural buckling resistance $N_{b,AISC,Rd}$ of homogeneous welded I-section columns with nominal yield strengths up to 690 N/mm^2:

$$N_{b,AISC,Rd} = \phi_c \chi_{AISC} A f_y \text{, for non-slender welded I-section columns} \quad (11)$$

in which ϕ_c is the resistance factor for member buckling resistances (equivalent to the inverse of the EC3 partial safety factor γ_{M1} in Eq. (8)), which has a recommended value of 0.9 in [15], and χ_{AISC} is the AISC flexural buckling reduction factor, which can be determined from a two-stage column buckling curve as expressed by Eq. (12).

$$\chi_{AISC} = \begin{cases} 0.658^{\bar{\lambda}^2} & \text{for } \bar{\lambda} \le 1.5 \\ \dfrac{0.877}{\bar{\lambda}^2} & \text{for } \bar{\lambda} > 1.5 \end{cases} \tag{12}$$

Similar to the EC3 design provisions, the American Specification AISC 360 [15] does not provide specific design rules for hybrid welded I-section columns failing by in-plane flexural buckling. In this subsection, the applicability of the two-stage column buckling curve to hybrid welded I-section columns is also assessed, with the weighted average yield strength $f_{y,a}$ given by Eq. (4) used for the calculation of the non-dimensional member slenderness $\bar{\lambda}$ (using Eq. (3)) and the AISC flexural buckling resistance (using Eq. (11)). The test and FE ultimate buckling resistances $N_{u,test/FE}$ are compared with the unfactored AISC resistance predictions $N_{u,AISC}$ in Fig. 18 and Table 8. It is shown that although the AISC design method generally leads to accurate resistance predictions for both homogeneous and hybrid welded I-section columns made of HSS grades, it provides unsafe predictions for welded I-section columns made of lower steel grades, especially for those buckling about the minor axis. The varying levels of accuracy of the AISC design method for welded I-section columns with different steels grades would be expected since the AISC 360 [15] adopts a single column buckling curve for welded I-section columns failing by in-plane flexural buckling about either axes, thus ignoring the influence of both the axis of buckling and the steel grade on the flexural buckling resistance of welded I-section columns.

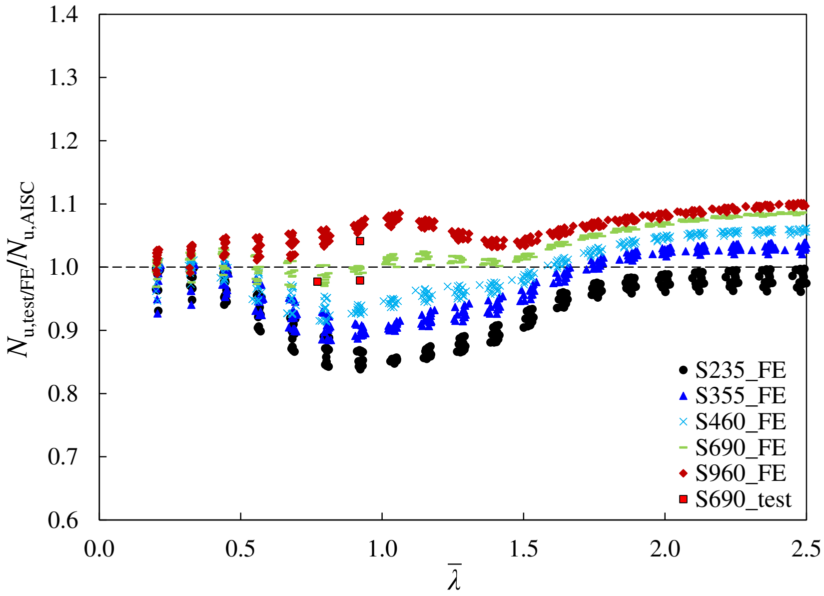

(a) Homogeneous welded I-section columns buckling about the major axis

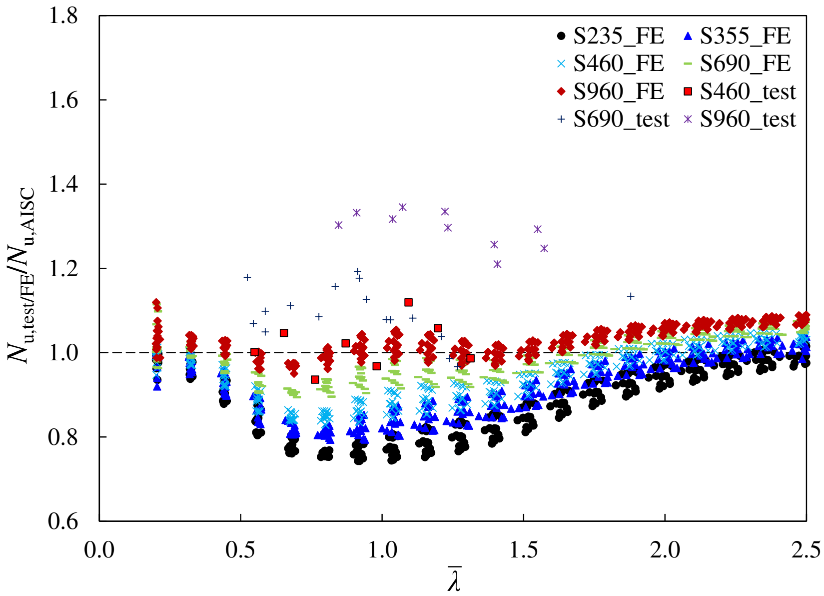

(b) Homogeneous welded I-section columns buckling about the minor axis

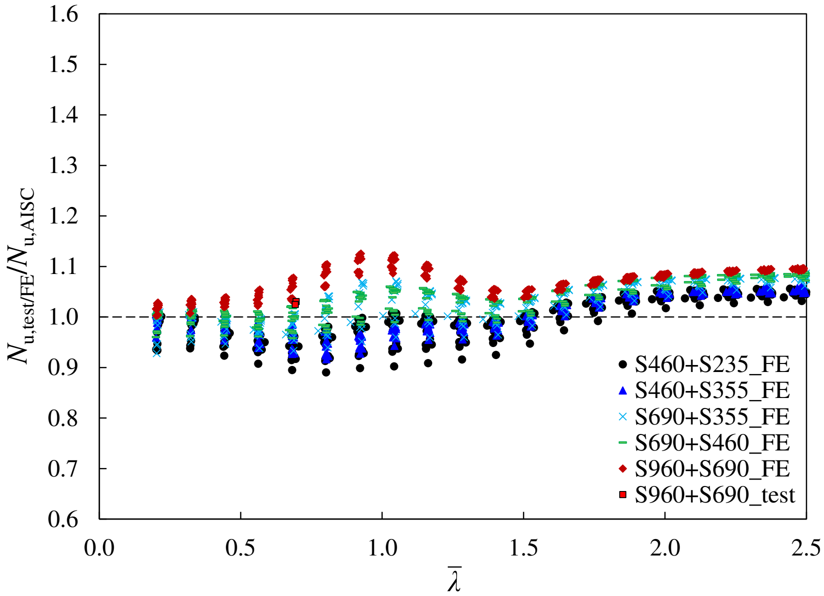

(c) Hybrid welded I-section columns buckling about the major axis

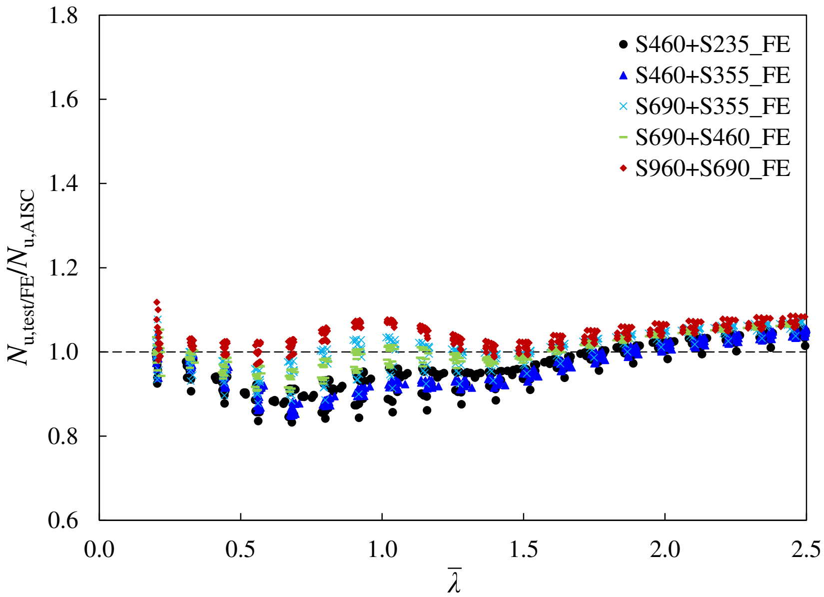

(d) Hybrid welded I-section columns buckling about the minor axis

Fig. 18. Comparisons of test and FE ultimate resistances of column specimens with those predicted using AISC 360 [15]

5.4. New design proposals

On the basis of the above assessments, it is generally found that the existing design rules of prEN 1993-1-1 [14] and AISC 360 [15] have scope for improvement in the flexural buckling resistance prediction of homogeneous and hybrid welded I-section columns made of varying steel grades. Welded I-section columns generally exhibit superior normalised column buckling resistances with increasing yield strength; this is attributed to the reducing relative influence of the initial imperfections, including both the residual stresses and the initial global geometric imperfections. Specifically, the residual stresses in welded I-sections have been found to reduce as a proportion of the yield strength with increasing steel grades, as described in Section 2, while the amplitudes of global geometric imperfections for columns with a given non-dimensional member slenderness $\bar{\lambda}$ decrease with increasing yield strength since the initial geometric imperfection is conventionally considered to be proportional to the column member length (e.g. L/1000) [16]. Therefore, to improve the accuracy and consistency of the design method, the influence of the steel grade (i.e. yield strength) on the flexural buckling resistance of welded I-section columns should be rationally considered.

New proposals for the flexural buckling design of homogeneous and hybrid welded I-section columns are developed herein on the basis of the current EC3 design rules. The design proposals feature modified imperfection factors $\alpha_{\text{mod-EC3}}$ for homogeneous and hybrid welded I-section columns as given by Eqs. (13) and (14) for major and minor axis flexural buckling, respectively, and a shortened buckling curve plateau length of $\bar{\lambda}_{0,\text{mod-EC3}} = 0.1$ for both homogeneous and hybrid welded I-section columns buckling about either axes, leading to a modified EC3 flexural buckling reduction factor $\chi_{\text{mod-EC3}}$, as described by Eqs. (15) and (16). Note that the modified imperfection factors $\alpha_{\text{mod-EC3}}$ are expressed in term of the flange material parameter $\varepsilon_{\text{f}} = \sqrt{235/f_{\text{y,f}}}$ since the flanges are decisive in their contribution to the flexural buckling resistance of welded I-section columns.

$$\alpha_{\text{mod-EC3}} = 0.45\varepsilon_{\text{f}}\text{, for flexural buckling about the major axis} \quad (13)$$

$$\alpha_{\text{mod-EC3}} = 0.55\varepsilon_{\text{f}} \text{, for flexural buckling about the minor axis} \quad (14)$$

$$\chi_{\text{mod-EC3}} = \frac{1}{\phi_{\text{mod-EC3}} + \sqrt{\phi_{\text{mod-EC3}}^2 - \bar{\lambda}^2}} \text{ but } \chi_{\text{mod-EC3}} \le 1.0 \quad (15)$$

$$\phi_{\text{mod-EC3}} = 0.5\left(1 + \alpha_{\text{mod-EC3}}\left(\bar{\lambda} - \bar{\lambda}_{0,\text{mod-EC3}}\right) + \bar{\lambda}^2\right) \quad (16)$$

The accuracy of the newly proposed flexural buckling curves for homogeneous and hybrid welded I-section columns is graphically examined in Fig. 19, in which the ratios of the test and FE column flexural buckling resistances to the resistance predictions using the proposed modified EC3 design approach $N_{\text{u,test/FE}}/N_{\text{u,mod-EC3}}$ are plotted against the non-dimensional member slenderness $\bar{\lambda}$. The normalised data points are seen to display a significantly tighter (i.e. less scattered) trend compared to the EC3 and AISC 360 predictions for both the homogeneous and hybrid welded I-section columns buckling about either axes, indicating that the influence of yield strength on the flexural buckling resistances of welded I-section columns is successfully captured by using the modified flexural buckling curves. The improvements offered by the proposed design rules over the current design methods in terms of accuracy and consistency are also confirmed by the statistical results summarised in Table 8.

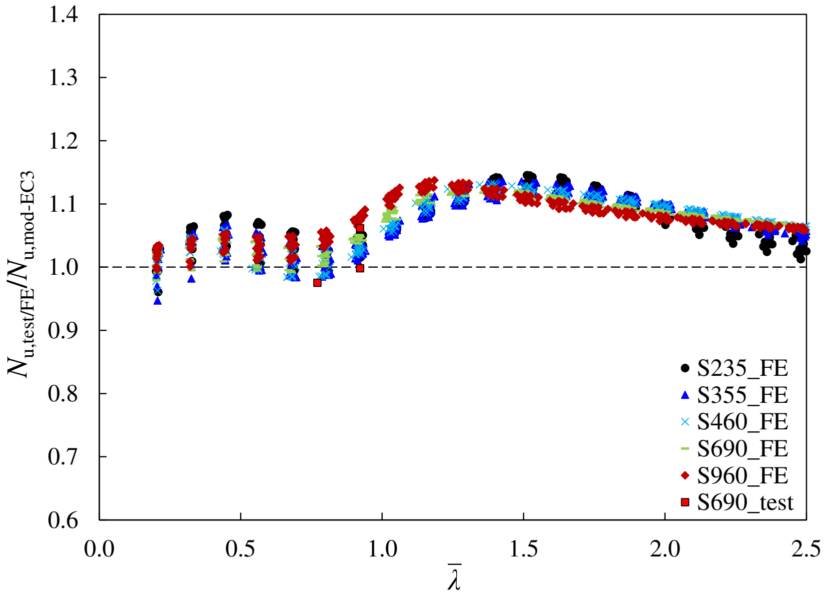

(a) Homogeneous welded I-section columns buckling about the major axis

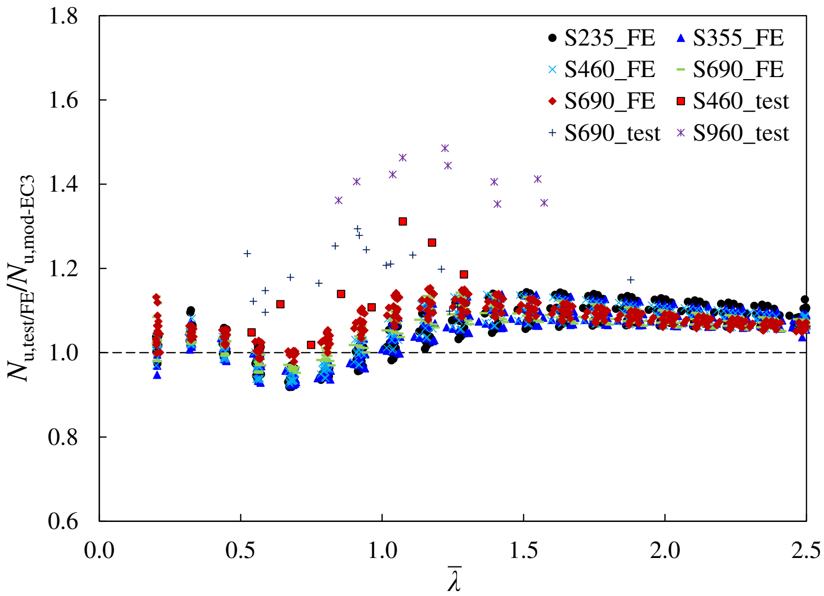

(b) Homogeneous welded I-section columns buckling about the minor axis

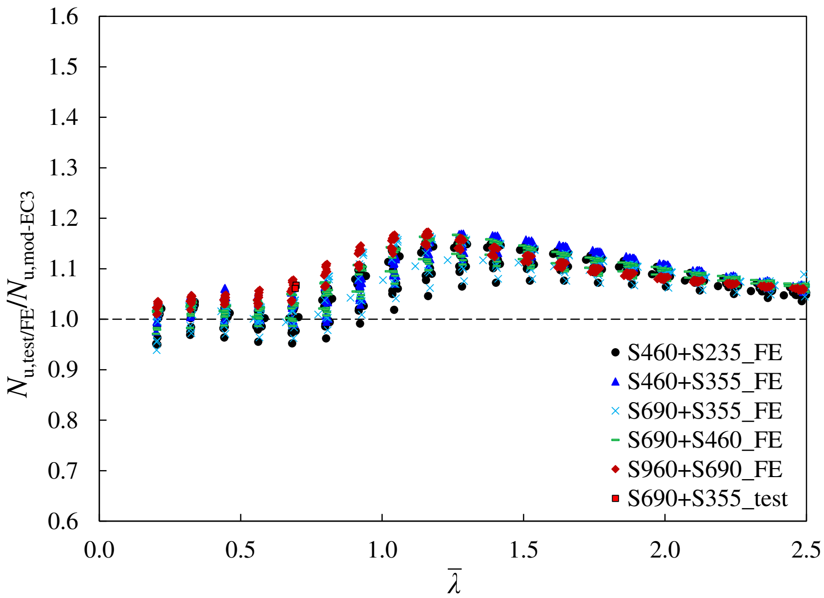

(c) Hybrid welded I-section columns buckling about the major axis

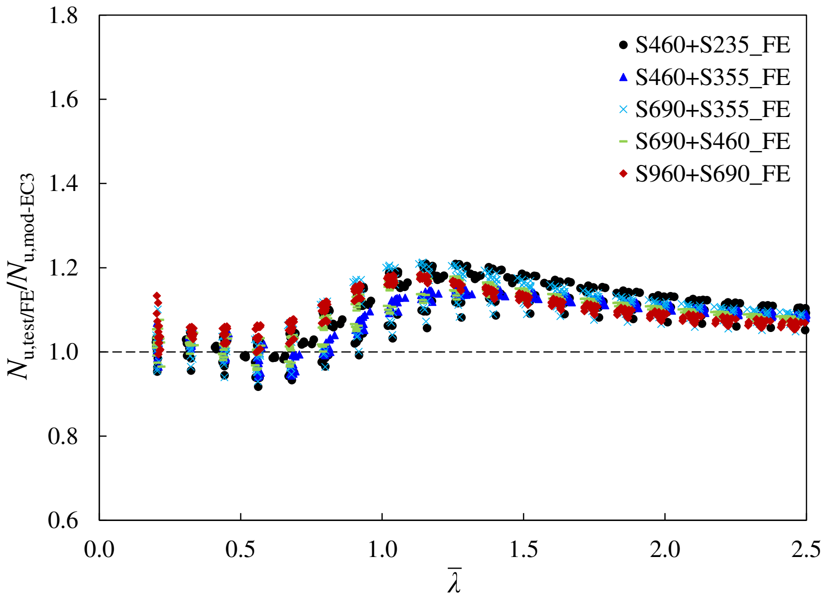

(d) Hybrid welded I-section columns buckling about the minor axis

Fig. 19. Comparisons of test and FE ultimate resistances of column specimens with those predicted using the new design proposals

6. Reliability analysis

In order to quantify the level of reliability of the existing and proposed buckling design approaches for the homogeneous and hybrid welded I-section columns, statistical analyses were performed following the guidance provided in EN 1990 [63]. The variability of the basic geometric and material properties was initially considered. For the welded I-sections, the mean and variability of the key cross-sectional dimensions, including H, B, t_f and t_w, were taken in accordance with Annex E of prEN 1993-1-1 [14], as presented in Table 9, where X_m/X_n is the ratio between the mean and nominal values of a property X and V_X is the corresponding coefficient of variation (COV). The COV of the cross-sectional area A, denoted by V_A, was utilised to represent the combined variability of the cross-sectional dimensions. The value of V_A was derived based on the COV values of the individual dimensions following the procedure set out by Afshan et al. [64]. Note that V_A varies slightly between cross-section profiles, but an average value of $V_A = 0.022$ for the range of considered welded I-sections was employed herein. The mean and variability of the key material properties, i.e. f_y and E, were also taken as those specified in prEN 1993-1-1 [14], as listed in Table 9.

Table 9. Mean and COV values of basic material and geometric parameters for welded I-sections in accordance with prEN 1993-1-1 [14]

Parameter	X_m / X_n	COV
H	1.00	0.009
B	1.00	0.009
t_f	0.98	0.025
t_w	1.00	0.025
f_y (S355, S420)	1.20	0.050
f_y (S460)	1.15	0.045
f_y (above S460)	1.10	0.035
E	1.00	0.030

The combined COV of the geometric and material parameters V_{rt} was subsequently derived as follows. The resistance function was first generalised into Eq. (17), where the exponents C_1, C_2 and C_3 describe the dependences of the resistance function on f_y, A and E respectively. The values of the C_i parameters were derived for each considered test and FE simulation following the approach described in [65], and the value of V_{rt} was then calculated using Eq. (18).

$$N_{\mathrm{b,R}} = C_0 f_{\mathrm{y}}^{C_1} A^{C_2} E^{C_3} \tag{17}$$

$$V_{\mathrm{rt}} = \sqrt{\left(C_1 V_{fy}\right)^2 + \left(C_2 V_A\right)^2 + \left(C_3 V_E\right)^2} \tag{18}$$

By comparing the experimental (or numerical) results $r_{\mathrm{e,i}}$ with the design predictions $r_{\mathrm{t,i}}$, the correction factor b and the COV of the errors V_{δ} were derived. Note that b was determined using Eq. (19) instead of the least squares method specified in EN 1990 [63], as recommended in [66]. The considered test and FE data population was divided into subsets based on the steel grades and relative slenderness to avoid overestimating the scatter, and the values of b and V_{δ} were calculated based on these subsets. The design fractile factor $k_{\mathrm{d,n}}$ was taken based on the total number of the data points in the original population, as recommended in EN 1990 [63].

$$b = \frac{1}{n}\sum_{i=1}^{n} \frac{r_{\mathrm{e,i}}}{r_{\mathrm{t,i}}} \tag{19}$$

Finally, the required partial safety factors, denoted by γ_{M1}^{*}, were derived, and the results are summarised, along with the other key statistical results from the reliability analyses, in Table 10 and 11 for the EC3 and proposed design approaches respectively. Note that the value of V_{r} varied with each considered test or FE data point, and the average values are shown in Tables 10 and 11. In general, the proposed design approach demonstrated a similar level of reliability to the existing EC3 approach, while improving the accuracy and consistency of the resistance predictions, as revealed previously in Section 5. Therefore, the proposed design rules are deemed suitable for inclusion into Eurocode 3 for the buckling design of welded homogeneous and hybrid I-section columns.

Table 10. Reliability analysis results for EC3 design approach

Column type	Buckling axis	Number of data points FE (test)	$k_{d,n}$	b	V_δ	V_r	γ^*_{M1}
Homogeneous welded I-section	Major	1500 (3)	3.097	1.061	0.070	0.054	1.061
Homogeneous welded I-section	Minor	1500 (35)	3.097	1.088	0.104	0.058	1.059
Hybrid welded I-section	Major	1500 (2)	3.097	1.091	0.069	0.056	1.050
Hybrid welded I-section	Minor	1500 (0)	3.097	1.132	0.080	0.058	1.024

Table 11. Reliability analysis results for proposed design approach

Column type	Buckling axis	Number of data points FE (test)	$k_{d,n}$	b	V_δ	V_r	γ^*_{M1}
Homogeneous welded I-section	Major	1500 (3)	3.097	1.071	0.039	0.054	1.035
Homogeneous welded I-section	Minor	1500 (35)	3.097	1.062	0.062	0.058	1.062
Hybrid welded I-section	Major	1500 (2)	3.097	1.075	0.047	0.055	1.051
Hybrid welded I-section	Minor	1500 (0)	3.097	1.077	0.050	0.055	1.054

7. Conclusions

The flexural buckling behaviour and design of both homogeneous and hybrid welded I-section columns of varying steel grades have been investigated in this paper. The amplitudes and distributions of residual stresses in homogeneous and hybrid S235 to S960 steel welded I-sections were firstly analysed on the basis of existing experimental data collected from the literature, and a new residual stress model with different statistical characterizations (mean and characteristic) was proposed. An experimental programme was then carried out to generate underpinning test data on both homogeneous and hybrid welded I-section columns failing by in-plane flexural buckling about the major axis. The experimental programme comprised tensile coupon tests, initial global geometric imperfection measurements and five pin-ended major axis flexural buckling tests. Three different welded I-section profiles were investigated in the experimental programme − two homogeneous welded I-sections with different geometries made of S690 steel and one hybrid welded I-section with S690 steel flanges and an S355 steel web.

Following the experimental programme, a comprehensive numerical investigation was performed, in which FE models were initially developed and validated against the flexural buckling test results on welded I-section columns generated in the present study and collected from the literature, and then used to conduct parametric studies to broaden the range of available flexural buckling data on homogeneous and hybrid welded I-section columns. In total, 6000 numerical data − 3000 on homogeneous welded I-section columns and 3000 on hybrid welded I-section columns, were generated, covering a variety of steel grades, cross-section geometries and member slendernesses. Based on the established test and FE database, the accuracy and applicability of the relevant codified design rules, as specified in prEN 1993-1-1 [14] and AISC 360 [15], were assessed. It was shown that the current design provisions yield somewhat scattered buckling resistance predictions. A new design approach based on the current EC3 design rules was then proposed, where the influence of the yield strength on the flexural buckling resistances of homogeneous and hybrid welded I-section columns was more rationally captured by using a yield strength-dependent imperfection factor. The proposed method was shown to offer a higher degree of accuracy and consistency in the predictions of flexural buckling resistances for both homogeneous and hybrid welded I-section columns with varying steel grades. Reliability analysis was finally conducted for the proposed design method in accordance with EN 1990 [63], indicating that the current EC3 partial safety factor of unity can be safely employed with the proposed method for the design of both homogeneous and hybrid welded I-section columns failing by in-plane flexural buckling. Further research on the flexural buckling behaviour and design of Class 4 (slender) welded I-section columns, which are greatly affected by the interaction of local and global buckling, as well as flexural-torsional buckling behaviour of HSS homogeneous and hybrid welded I-section columns are recommended.

Acknowledgements

This project has received funding from the Research Fund for Coal and Steel under grant agreement no. 743504. The authors would also like to thank Mr. Les Clark for his assistance and advice during the execution of this project.

References

[1] Deng Y, Zhou S, Li J, Nie S, Liu P. Buckling behaviour of Q460GJ welded H-section columns subjected to minor axis under axial compression. Structures 2021;34:1416-1428.

[2] Ban H, Shi G, Shi Y, Bradford MA. Experimental investigation of the overall buckling behaviour of 960 MPa high strength steel columns. J Constr Steel Res 2013;88:256-266.

[3] Su A, Liang Y, Zhao O. Experimental and numerical studies of S960 ultra-high strength steel welded I-section columns. Thin-Wall Struct 2021;159:107166.

[4] Li TJ, Li GQ, Chan SL, Wang YB. Behavior of Q690 high-strength steel columns: Part 1: Experimental investigation. J Constr Steel Res 2016;123:18-30.

[5] Shi G, Ban H, Bijlaard FS. Tests and numerical study of ultra-high strength steel columns with end restraints. J Constr Steel Res 2012;70:236-247.

[6] Ban H, Shi G. Overall buckling behaviour and design of high-strength steel welded section columns. J Constr Steel Res 2018;143:180-195.

[7] Ito M, Nozaka K, Shirosaki T, Yamasaki K. Experimental study on moment-plastic rotation capacity of hybrid beams. J Bridge Eng 2005;10(4):490-496.

[8] Wang CS, Duan L, Chen YF, Wang SC. Flexural behavior and ductility of hybrid high performance steel I-girders. J Constr Steel Res 2016;125:1-14.

[9] Bartsch H, Eyben F, Pauli G, Schaffrath S, Feldmann M. Experimental and numerical investigations on the rotation capacity of high-strength steel beams. J Struct Eng

2021;147(6):04021067.

[10] Nethercot DA. Buckling of welded hybrid steel I-beams. J Struct Div 1976, 102(3), 461-474.

[11] Shokouhian M, Shi Y. Flexural strength of hybrid steel I-beams based on slenderness. Eng Struct 2015;93:114-128.

[12] EN 1993-1-1:2005. Eurocode 3: Design of steel structures – Part 1-1: General rules and rules for buildings. European Committee for Standardization (CEN), Brussels; 2005.

[13] EN 1993-1-12:2007. Eurocode 3: Design of steel structures – Part 1-12: Additional rules for the extension of EN 1993 up to steel grades S700. European Committee for Standardization (CEN), Brussels; 2007.

[14] prEN 1993-1-1:2019. Eurocode 3: Design of steel structures – Part 1-1: General rules and rules for buildings. European Committee for Standardization (CEN), Brussels; 2005.

[15] AISC 360-16, Specification for structural steel buildings, American Institute of Steel Construction (AISC), Chicago, Illinois, 2016.

[16] Meng X, Gardner L. Behavior and design of normal-and high-strength steel SHS and RHS columns. J Struct Eng 2020;146(11):04020227.

[17] Yun X, Meng X, Gardner L. Design of cold-formed steel SHS and RHS beam–columns considering the influence of steel grade. Thin-Wall Struct 2022;171:108600.

[18] Wang YB, Li GQ, Chen SW. Residual stresses in welded flame-cut high strength steel H-sections. J Constr Steel Res 2012;79:159-65.

[19] Le T, Paradowska A, Bradford MA, Liu X, Valipour HR. Residual stresses in welded high-strength steel I-Beams. J Constr Steel Res 2019:105849.

[20] Liu X, Chung KF. Experimental and numerical investigation into temperature histories and residual stress distributions of high strength steel S690 welded H-sections. Eng Struct 2018;165:396-411.

[21] Li TJ, Li GQ, Wang YB. Residual stress tests of welded Q690 high-strength steel box- and H-sections. J Constr Steel Res 2015;115:283-89.

[22] Tankova T, Simões da Silva L, Balakrishnam M, Rodrigues D, Launert B, Pasternak H, Tun TY. Residual stresses in welded I section steel members. Eng Struct 2019;197:109398.

[23] Schaper L, Tankova T, da Silva LS, Knobloch M. A novel residual stress model for welded I-sections. J Constr Steel Res 2022;188:107017.

[24] Wang W, Qin S. Experimental investigation of residual stresses in thin-walled welded H-sections after fire exposure. Thin-Walled Struct 2016;101:109–119.

[25] Shiomi H, Kurata M. Strength Formula for Tapered Beam-Columns. J Struct Eng 1984;110:1630–1643.

[26] Unsworth D, Driver RG, Li L. Measurement and prediction of residual stresses in welded girders. J Constr Steel Res 2020;169:106007.

[27] Yang B, Nie S, Kang SB, Xiong G, Hu Y, Bai J, et al. Residual stress measurement on welded Q345GJ steel H-sections by sectioning method and method improvement. Adv Steel Constr 2017;13:78–95.

[28] Schaper L, Jörg F, Winkler R, Kuhlmann U, Knobloch M. The simplified method of the equivalent compression flange: Development based on LTB tests and residual stress measurements. Steel Constr 2019;12:264–277.

[29] Ban H, Shi G, Bai Y, Shi Y, Wang Y. Residual stress of 460 MPa high strength steel welded i section: Experimental investigation and modeling. Int J Steel Struct 2013;13:691–705.

[30] Yang B, Nie S, Xiong G, Hu Y, Bai J, Zhang W, et al. Residual stresses in welded I-shaped sections fabricated from Q460GJ structural steel plates. J Constr Steel Res 2016;122:261–273.

[31] Tankova T, Rodrigues F, Leitão C, Martins C, Simões da Silva L. Lateral-torsional buckling of high strength steel beams: Experimental resistance. Thin-Walled Struct 2021;164:107913.

[32] Zhao J, Ding W. Tests and design method on overall buckling behaviours of welded I-section two-span continuous beams for Q460 high strength steel. Eng Struct 2022;253:113789.

[33] Sun Y, Liang Y, Zhao O. Testing, numerical modelling and design of S690 high strength steel welded I-section stub columns. J Constr Steel Res 2019;159:521–533.

[34] Su A, Sun Y, Liang Y, Zhao O. Material properties and membrane residual stresses of S690 high strength steel welded I-sections after exposure to elevated temperatures. Thin-Walled Struct 2020;152:106723.

[35] Ban H Y. Research on the overall buckling behavior and design method of high strength steel columns under axial compression. Ph. D. thesis, Tsinghua Univ., Beijing (in Chinese), 2012.

[36] ECCS. Ultimate limit state calculation of sway frames with rigid joints. 1st ed. P033.ECCS technical committee 8 – structural stability. Brussels: European Convention of Constructional Steel Work; 1984.

[37] prEN 1993-1-14, Eurocode 3: Design of Steel Structures – Part 1-14: Design By FE Analysis, European Committee for Standardization (CEN), Brussels, 2019.

[38] Shayan S, Rasmussen KJR, Zhang H. Probabilistic modelling of residual stress in advanced analysis of steel structures. J Constr Steel Res 2014;101:407–414.

[39] Arrayago I, Rasmussen KJR, Real E. Statistical analysis of the material, geometrical and imperfection characteristics of structural stainless steels and members. J Constr Steel Res 2020;175:106378.

[40] Fieber A, Gardner L, Macorini L. Design of structural steel members by advanced inelastic analysis with strain limits. Eng Struct 2019;199:109624.

[41] Fieber A, Gardner L, Macorini L. Structural steel design using second-order inelastic analysis with strain limits. J Constr Steel Res 2020;168:105980.

[42] Gardner L, Yun X, Fieber A, Macorini L. Steel design by advanced analysis: material modeling and strain limits. Engineering 2019;5(2):243-249.

[43] Yun X, Zhu YF, Wang ZX, Gardner L. Benchmark tests on high strength steel frames. Eng Struct 2022;258(8):114108.

[44] Yun X, Gardner L. Stress-strain curves for hot-rolled steels. J Constr Steel Res 2017;133:36-46.

[45] Kyprianou C, Kyvelou P, Gardner L, Nethercot DA. Experimental study of sheathed cold-formed steel beam-columns. Thin-Walled Struct 2021;166:108044.

[46] Behzadi-Sofiani B, Gardner L, Wadee MA. Stability and design of fixed-ended stainless steel equal-leg angle section compression members. Eng Struct 2021;249:113281.

[47] Ziemian RD. Guide to stability design criteria for metal structures. John Wiley & Sons; 2010.

[48] Zhong, Y., Sun, Y., Zhao, O. and Gardner, L. (2022) Structural response and residual capacity of S700 high strength steel CHS columns after exposure to fire. Journal of Structural Engineering,

ASCE. 148(6), 04022050.

[49] ABAQUS V.6.21, Commercial FE Software and Documentation Dassault Systèmes, Simulia Corporation, Providence, RI, USA, 2021.

[50] Tse K, Wang J, Yun X. Structural behaviour and continuous strength method design of high strength steel non-slender welded I-section beam–columns. Thin-Wall Struct 2021;169:108273.

[51] Yun X, Gardner L, Boissonnade N. Ultimate capacity of I-sections under combined loading–Part 1: Experiments and FE model validation. J Constr Steel Res 2018;147:408-421.

[52] Bu Y, Gardner L. Laser-welded stainless steel I-section beam-columns: testing, simulation and design. Eng Struct 2019;179:23-36.

[53] Russell MJ, Lim JBP. Roy K, Clifton GC, Ingham JM. Welded steel beam with novel cross-section and web openings subject to concentrated flange loading. Structures 2020;24:580-599.

[54] Feng R, Liu J, Chen Z, Roy K, Chen B, Lim JBP. Numerical investigation and design rules for flexural capacities of H-section high-strength steel beams with and without web openings. Eng Struct 2020;225:111278.

[55] Schafer B, Ádány S. Buckling analysis of cold-formed steel members using CUFSM: conventional and constrained finite strip methods. Proceedings of the 18th International Specialty Conference on Cold-Formed Steel Structures, Orlando, FL, USA; 2006:39-54.

[56] Fieber A, Gardner L, Macorini L. Formulae for determining elastic local buckling half-wavelengths of structural steel cross-sections. J Constr Steel Res 2019;159:493-506.

[57] EN 1993-1-5:2006. Eurocode 3: Design of steel structures – Part 1-5: Plated structural elements. European Committee for Standardization (CEN), Brussels; 2006.

[58] EN 1090-2. Execution of steel structures and aluminium structures – Part 2: Technical requirements for steel structures. European Committee for Standardization (CEN), Brussels; 2018.

[59] Matlab. Version: R2020a, The MathWorks Inc., Natick, Massachusetts, 2020.

[60] Gardner L, Fieber A, Macorini L. Formulae for calculating elastic local buckling stresses of full structural cross-sections. Structures 2019;17:2-20.

[61] Baddoo N, Sansom M, Pimentel R, Lawson M, Chen A, Meza F, Gardner L, Yun X, Zhu Y, Schaffrath S, Bartsch H, Eyben F, da Silva LS, Tankova T, Rodrigues F, Lehnert T, Gong F, Durr

A. Stronger Steels in the Built Environment (STROBE), Final report, Research Fund for Coal and Steel, GA 743504, 2021.
[62] W. Ayrton, J. Perry, On struts, The Engineer 62 (1886) 1-55.
[63] EN 1990, Eurocode: Basis of structural design, European Committee for Standardization (CEN), Brussels, 2002.
[64] Afshan S, Francis P, Baddoo NR, Gardner L, Reliability analysis of structural stainless steel design provisions, J Constr Steel Res 2015;114:293-304.
[65] Meng X, Gardner L, Testing, modelling and design of normal and high strength steel tubular beam-columns J Constr Steel Res 2021;183:106735.
[66] Meng X, Gardner L, Sadowski AJ, Rotter JM, Elasto-plastic behaviour and design of semi-compact circular hollow sections Thin-Walled Struct 2020;148(6):106486.